Jupiter's Low-Altitude Auroral Zones: Fields, Particles, Plasma Waves, and Density Depletions

A. H. Sulaiman[1], B. H. Mauk[2], J. R. Szalay[3], F. Allegrini[4,5], G. Clark[2], G. R. Gladstone[4,5], S. Kotsiaros[6], W. S. Kurth[1], F. Bagenal[7], B. Bonfond[8], J. E. P. Connerney[9,10], R. W. Ebert[4,5], S. S. Elliott[11], D. J. Gershman[10], G. B. Hospodarsky[1], V. Hue[4], R. L. Lysak[11], A. Masters[12], O. Santolík[13,14], J. Saur[15], and S. J. Bolton[4]

[1]Department of Physics and Astronomy, University of Iowa, Iowa City, IA, USA, [2]Applied Physics Laboratory, Johns Hopkins University, Laurel, MD, USA, [3]Department of Astrophysical Sciences, Princeton University, Princeton, NJ, USA, [4]Southwest Research Institute, San Antonio, TX, USA, [5]Department of Physics and Astronomy, University of Texas at San Antonio, San Antonio, TX, USA, [6]DTU-Space, Technical University of Denmark, Kongens Lyngby, Denmark, [7]Laboratory for Atmospheric and Space Physics, University of Colorado Boulder, Boulder, CO, USA, [8]Space Sciences, Technologies and Astrophysics Research Institute, LPAP, Université de Liège, Liège, Belgium, [9]Space Research Corporation, Annapolis, MD, USA, [10]NASA/Goddard Space Flight Center, Greenbelt, MD, USA, [11]Minnetota Institute for Astrophysics, School of Physics and Astronomy, University of Minnesota, Minneapolis, MN, USA, [12]Blackett Laboratory, Imperial College London, London, UK, [13]Department of Space Physics, Institute of Atmospheric Physics of the Czech Academy of Sciences, Prague, Czechia, [14]Faculty of Mathematics and Physics, Charles University, Prague, Czechia, [15]Institute of Geophysics and Meteorology, University of Cologne, Cologne, Germany

Abstract The Juno spacecraft's polar orbits have enabled direct sampling of Jupiter's low-altitude auroral field lines. While various data sets have identified unique features over Jupiter's main aurora, they are yet to be analyzed altogether to determine how they can be reconciled and fit into the bigger picture of Jupiter's auroral generation mechanisms. Jupiter's main aurora has been classified into distinct "zones", based on repeatable signatures found in energetic electron and proton spectra. We combine fields, particles, and plasma wave data sets to analyze Zone-I and Zone-II, which are suggested to carry upward and downward field-aligned currents, respectively. We find Zone-I to have well-defined boundaries across all data sets. H^+ and/or H_3^+ cyclotron waves are commonly observed in Zone-I in the presence of energetic upward H^+ beams and downward energetic electron beams. Zone-II, on the other hand, does not have a clear poleward boundary with the polar cap, and its signatures are more sporadic. Large-amplitude solitary waves, which are reminiscent of those ubiquitous in Earth's downward current region, are a key feature of Zone-II. Alfvénic fluctuations are most prominent in the diffuse aurora and are repeatedly found to diminish in Zone-I and Zone-II, likely due to dissipation, at higher altitudes, to energize auroral electrons. Finally, we identify significant electron density depletions, by up to 2 orders of magnitude, in Zone-I, and discuss their important implications for the development of parallel potentials, Alfvénic dissipation, and radio wave generation.

1. Introduction

The combination of Jupiter's strong magnetic field, rapid rotation, and internally sourced mass loading creates a magnetosphere that is fundamentally different from its terrestrial counterpart. Structurally, the magnetosphere is inflated with the average observed distance of the magnetopause far greater than the expected distance predicted from the internal dipolar magnetic pressure standing off the external solar wind dynamic pressure (Joy et al., 2002). Mass loading of iogenic plasma in the magnetosphere at a widely assumed rate of ∼1 ton/s, primarily in the form of S and O (in various charge states), greatly enhances the internal pressure owing to centrifugal, thermal, and magnetic stresses, thereby pushing the magnetopause farther out. The action of these forces confines the heavy plasma into the equatorial region of Jupiter's magnetosphere as a thin current sheet, with varying thickness as a function of local time imposed by Jupiter's rotation (Khurana et al., 2004; Thomas et al., 2004).

Dynamically, conservation of angular momentum breaks down the corotation of iogenic plasma as it is transported radially outward. This introduces a significant azimuthal component to Jupiter's magnetic field, starting in the middle magnetosphere ($\gtrsim$10 R_J; 1 R_J = 71,492 km as Jupiter's equatorial radius). This large-scale configuration has been thought to be the framework for Jupiter's main auroral oval as a current system imparts the required

$\mathbf{J} \times \mathbf{B}$ force to enforce corotation (Cowley & Bunce, 2001; Hill, 1979; Kivelson & Southwood, 2005). Charge density continuity is satisfied by field-aligned currents and this is the basis upon which magnetosphere-ionosphere coupling is established. This steady-state picture has been modeled extensively to explain the observed brightness and location of Jupiter's main auroral oval (e.g., Nichols & Cowley, 2004; Ray et al., 2010) by citing a relationship between parallel potentials and field-aligned currents, originally developed for Earth's aurora (Knight, 1973). A consequence of this is a mono-energetic or peaked electron distribution as current-carrying electrons unidirectionally gain energy, $q\phi_{\parallel}$, proportional to the potential drop. A different approach put forth by Saur et al. (2002, 2003) emphasizes the importance of prevalent small-scale magnetic perturbations brought about by radial transport in Jupiter's magnetosphere. The authors hypothesized that Jupiter's magnetosphere-ionosphere coupling is inherently time-dependent and mediated by weak magnetohydrodynamic turbulence, whereby Alfvén waves nonlinearly interact with one another as they partially reflect off-density gradients. As these fluctuations undergo a turbulent cascade toward kinetic scales, wave dissipation takes place and stochastically accelerates electrons. The commonly observed broadband, bidirectional electron distributions in the low-altitude regions of Jupiter's aurora have brought to the fore the importance of the time-dependent nature of Jupiter's magnetosphere (e.g., Allegrini et al., 2017; Lysak et al., 2021; Mauk et al., 2017a, 2017b; Saur et al., 2018).

Prior to Juno's arrival, Jupiter's main aurora was investigated using remote observations and was found to be more powerful and less variable than Earth's aurora (e.g., Gladstone et al., 2002; Grodent et al., 2015; Waite et al., 2001). The principal difference is that Jupiter's aurora is primarily driven by the internal dynamics of its magnetosphere, whereas Earth's is primarily driven by the external solar wind (Cowley & Bunce, 2001; Hill, 2001). Recent modeling shows that most of the polar cap region is threaded by the magnetic flux that closes within the planet, while only a small crescent-shaped region of flux is "open" to the solar wind (Zhang et al., 2021). This is attributed to slow reconnection rates at the magnetopause relative to the timescale of planetary rotation, thereby limiting the amount of magnetic flux that can be open (Delamere & Bagenal, 2010; Masters, 2017, 2018; McComas & Bagenal, 2007).

The Juno spacecraft's low-perijove, polar orbits have enabled in-situ sampling of low-altitude magnetic field lines threading Jupiter's polar aurora (e.g., Allegrini et al., 2017; Kurth, Imai, et al., 2017; Mauk, Haggerty, Jaskulek, et al., 2017). Juno's instruments have made direct measurements of critical observables connected to the main aurora, namely the characteristics of precipitating electrons (e.g., Allergrini et al., 2020; Mauk et al., 2020), magnetic field perturbations (Gershman et al., 2019; Kotsiaros et al., 2019), radio and plasma wave emissions (e.g., Kurth, Imai, et al., 2017; Kurth et al., 2018; Louarn et al., 2017), as well as high-resolution ultraviolet (UV; e.g., Bonfond et al., 2017; Gladstone, Persyn, et al., 2017; Gladstone, Versteeg, et al., 2017) and infrared (e.g., Mura et al., 2017) imagery. Altogether, these afford the capability to examine the seemingly unique macro-physics and micro-physics sustaining Jupiter's aurora.

A key finding related to Jupiter's auroral particles is the often-observed broadband energetic field-aligned electrons with a power law extending into the MeV range and a lack of sharp peak in energy (Mauk et al., 2017a, 2017b, 2018). These electron beams can have energy fluxes exceeding 3 W/m^2 and exhibit bidirectionality that is more often asymmetric, with a systematically preferred direction depending on latitude (Mauk et al., 2020). This appears to be the dominant precipitating electron signature associated with the brightest aurora at Jupiter (Allergrini et al., 2020; Mauk et al., 2017b) and is in contrast with Earth's brightest aurora where they have been demonstrated to be powered by inverted V distributions set up by parallel potentials (Carlson et al., 1998; Ergun et al., 1998a). The more familiar peaked energy distributions in the form of inverted V electron and ion distributions have also been observed by Juno, indicating that large-scale parallel electric potentials also play a role (Clark et al., 2017, 2018). Although these two phenomena are disparate in nature, they are believed to be closely associated with one another and have both been identified to operate together in a single auroral zone as defined by Mauk et al. (2020) and summarized below.

Using the Jupiter Energetic-particle Detector Instrument (JEDI) instrument (described in the next section) with orbits favoring the duskside, Mauk et al. (2020) classified Jupiter's main aurora into three distinct zones, two of which will be the focus of this work. These are Zone-I and Zone-II, comprising regions of the aurora dominated by persistent and repeatable signatures of field-aligned energetic electrons.

1. Zone-I (ZI): At the intermediate latitudes of the main auroral oval, this is characterized by more intense electron populations within the downward loss cone than outside, and with greater downward electron intensities and energy fluxes than upward.

2. Zone-II (ZII): At the higher latitudes, this is characterized by more intense electron populations within the upward loss cone than outside, and with greater or equal upward electron intensities and energy fluxes than downward. Here, remarkably, the downward fluxes are nevertheless sufficient to cause observable and powerful auroral intensities.

Zone-I and Zone-II have been suggested to be associated with upward and downward electric currents, respectively, for a single event (Mauk et al., 2020). Equatorward of these zones is the diffuse aurora (DifA), characterized by more intense high-energy electron populations outside of the loss cone than within, and with greater downward electron intensities and energy fluxes than upward.

Poleward of the zones is the polar cap—a vast and dynamic region where persistent highly field-aligned, upgoing energetic electrons have been observed (both inverted V and broadband distributions, albeit spatially separated) simultaneously with upgoing broadband emissions interpreted as the whistler mode (Ebert et al., 2017; Elliott, Gurnett, Kurth, Clark, et al., 2018; Elliott, Gurnett, Kurth, Mauk, et al., 2018; Mauk et al., 2020; Paranicas et al., 2018). There has been ongoing research on plasma processes in this region and this will not be the focus of this study (e.g., Elliott et al., 2020; Masters et al., 2021; Shi et al., 2020; Szalay et al., 2022).

In this study, we combine all four instruments (described in the next section) from Juno's fields and particles package to reconcile the various repeatable features exhibited by particle spectra, electric and magnetic field spectra, as well as field-aligned currents across Jupiter's auroral zones.

2. Instruments and Data Description

We utilize four in-situ instruments onboard Juno with fields-measuring and particles-measuring capabilities.

The Waves instrument measures an electric field component, E_y, using a 4.8-m tip-to-tip electric dipole antenna that is parallel to the spacecraft y-axis (Kurth, Hospodarsky, et al., 2017). Its containment within the spin (x-y) plane means two electric field components are effectively measured twice per spin with a period of 30 s. A magnetic search coil measures a magnetic field component, B_z, using a single sensor mounted along the spacecraft's spin (z) axis. We utilize Waves data provided by the Low-Frequency Receiver which covers the frequency ranges of 50 Hz to 20 kHz simultaneously for the E-fields and B-fields at 50 kilosamples per second. This frequency range is sufficient to capture plasma waves well below and above and the proton cyclotron frequency, f_{cH+}, in the near-Jupiter environment, by virtue of the very high magnetic field strength.

The Waves suite provides the capability to distinguish between electrostatic, $\delta E(f) \gg c\delta B(f)$, and electromagnetic, $\delta E(f) \sim c\delta B(f)$, waves below 20 kHz. Furthermore, the Poynting vector direction at a given frequency, $\delta\vec{E}(f) \times \delta\vec{B}(f)/\mu_0$, can be resolved, although incomplete measurement of all three E-field and three B-field components means some assumptions are necessary. We mitigate this issue by reasonably assuming that the plasma waves are propagating either almost parallel or anti-parallel to $\vec{B_0}$. Only one component of the Poynting vector can be resolved, which is along the spacecraft x-axis and its sign is compared with the sign of the background magnetic field's x-component, B_{0x}. The sign of the Poynting vector component is determined from the mutual phases between E_y and B_z, with the mutual phases $\phi_{Ey\text{-}Bz}$ and coherency, $C_{Ey\text{-}Bz}$ calculated. In the northern hemisphere, the combination of $\phi_{Ey\text{-}Bz} \approx 0°$ (180°) and a positive B_{0x} indicates upgoing (downgoing) plasma waves, that is, away from (toward) Jupiter. The reverse is true when either B_{0x} is negative or the spacecraft is in the southern hemisphere. This technique has been used at Jupiter to constrain the direction of lightning-induced rapid whistlers (Kolmašová et al., 2018), plasma waves in Jupiter's aurora (Kurth et al., 2018), as well as Io's Main Alfvén Wing (Sulaiman et al., 2020).

The JEDI measures energetic charged particle distributions. For this study, we utilize JEDI's 50–1,000 keV electron-measuring and 50 keV to >2,000 keV proton-measuring capabilities. The Jovian Auroral Distributions Experiment (JADE) measures thermal charged particle distributions. We utilize JADE's 3–30 keV electron (JADE-E) and 0.5–46 keV/q ion (JADE-I) sensors for H^+. JADE and JEDI complement one another to provide electron and proton energy and pitch angle spectra over a wide energy range. More details on the instruments can be found in Mauk et al. (2017) and McComas et al. (2017), respectively. Science-ready data techniques and challenges are detailed in Mauk et al. (2020) and Allegrini et al. (2020, 2021).

For the purpose of this study, we calculate the energy flux for electrons and H^+ (see Allergrini et al., 2020; Clark et al., 2018; Mauk et al., 2017). This is given by

$$Energy\,Flux = \pi \int_{E_{min}}^{E_{max}} I \cdot E\,dE \qquad (1)$$

where I is the particle intensity (cm^{-2} s^{-1} sr^{-1} keV^{-1}), E is the electron energy (keV) and π is the area-projected-weighted size of the loss cone. The width of the loss cone is estimated as $arcsin(1/R^3)^{1/2}$, where R is the Jovicentric distance in Jovian radii.

The fluxgate magnetometer (MAG) measures three components of the magnetic field and is used to determine the direction of field-aligned currents inferred from azimuthal deflections in the magnetic field, δB_ϕ (Connerney et al., 2017). This is achieved by subtracting the modeled internal planetary field (Connerney et al., 2018) and slowly varying trends from the measurements, leaving out the deflections. The very high field strength compared to the average size of the deflections associated with the auroral currents poses challenges and this technique is thoroughly discussed by Kotsiaros et al. (2019). Furthermore, measured magnetic field fluctuations can be transformed into transverse and compressive components to identify the presence of Alfvén waves (Gershman et al., 2019). In our analysis, M-shells (magnetic shells for non-dipolar magnetic fields (McIlwain, 1961)) were calculated by field-line tracing using the JRM09 internal field model (Connerney et al., 2018) with a superimposed external current sheet model (Connerney et al., 1981).

The magnetic field measurements allow JADE and JEDI to order particle counts by pitch angle, thus allowing for particle direction to be determined. Furthermore, the magnetic field strength is used by Waves to calculate the electron and proton cyclotron frequencies, f_{ce} and f_{cH+}, and this allows for the species' temporal scales to be identified in spectrograms.

This study highlights data sets taken from the early part of *Juno*'s Prime Mission phase when the spacecraft's orbital plane was in the dawn sector (thereby sampling the dusk aurora near perijove). This is due to the approximate orthogonality between Jupiter's magnetic field and *Juno*'s spin vectors, which optimizes pitch angle coverage. The pitch angle coverage was compromised as *Juno*'s orbital plane migrated toward the nightside and will begin to improve as the migration continues into the dusk sector (and sample the dawn aurora near perijove) in the Extended Mission phase.

3. Overview of Fields, Particles, and Plasma Waves in Jupiter's Auroral Zones

We begin by providing an overview of the various fields, particles, and plasma wave phenomena observed when Juno was magnetically connected to (and equatorward of) Jupiter's auroral zones. We analyze four auroral passes which are shown in Figure 1 as UV images from the Ultraviolet Spectrograph instrument (Gladstone, Persyn, et al., 2017; Gladstone, Versteeg, et al., 2017) with Juno's magnetic footprint track overlaid. Figure 2 shows multi-instrument data sets recorded during Juno's pass of Jupiter's southern aurora after its fourth perijove (PJ4S) corresponding to the aurora shown in Figure 1a. Figures 2a and 2b are electric and magnetic field frequency-time spectrograms, respectively, with the H^+ and H_3^+ cyclotron frequency, f_{cH+} and f_{cH3+}, overlaid. Throughout the time interval, f_{cH+} and f_{cH3+} were well within the frequency range of the Low-Frequency Receiver (50–20,000 Hz). Such strong magnetic fields have not been previously met by spacecraft. Particularly for sampling auroral field lines, the strength of Jupiter's magnetic field allows the Waves instrument to detect plasma waves at frequencies below f_{cH+} and f_{cH3+}, and thus analyze interactions with protons and heavy ions. Figure 2c is a spectrogram of the transverse (non-compressive) magnetic field power recorded by the MAG between 0.2 and 5 Hz (Gershman et al., 2019). Overlaid is the perturbation of Jupiter's azimuthal magnetic field, δB_φ, after subtracting the JRM09 internal field model (Connerney et al., 2018). From Ampère's law, significant gradients in the δB_φ perturbations are diagnostic of field-aligned currents (e.g., Kotsiaros et al., 2019). Figure 2d is a time series of the electron energy flux for the lower (3–30 keV) and higher (50–1,000 keV) energy ranges recorded by JADE and JEDI, respectively. These are specifically for populations within the loss cone and are differentiated between upward (away from Jupiter) and downward (toward Jupiter). Similarly, Figure 2e is a time series of the H^+ energy flux covering lower (0.5–50 keV) and higher (50–2,600 keV) energy ranges within the loss cone recorded by JADE and JEDI, respectively.
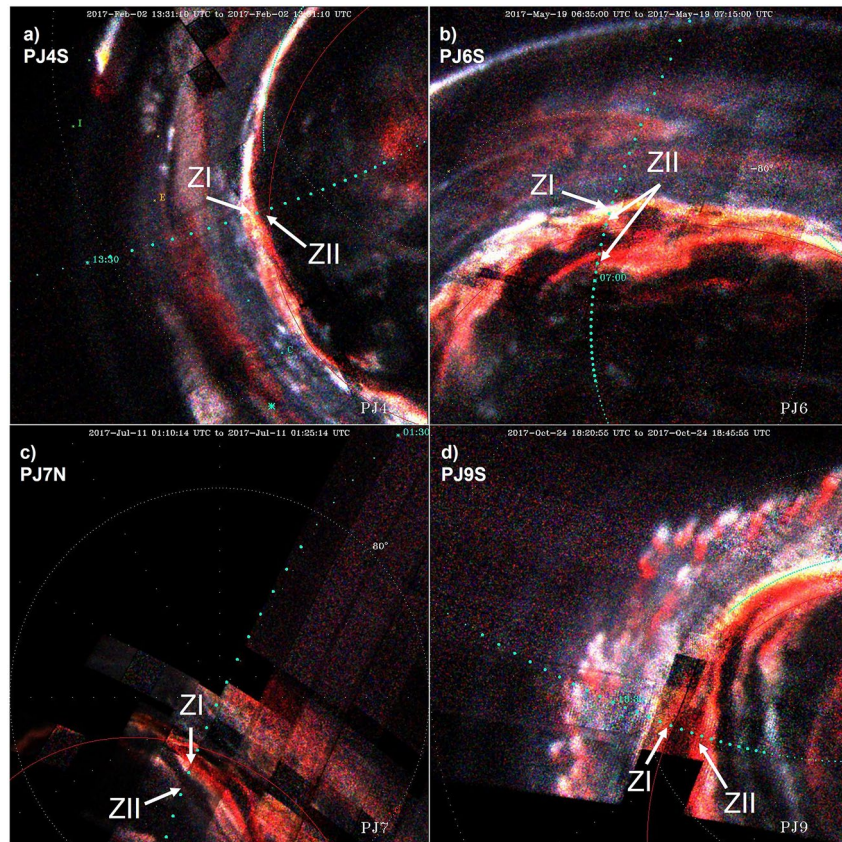
Figure 1. Orthographic projections of ultraviolet images of Jupiter's aurora in false color for each event presented in Figures 2–5. Overlaid are magnetic footprint tracks of Juno separated by 1 min. Colorbar can be found in Figure S1 of Supporting Information S1.

Describing the PJ4S data from left to right along Juno's poleward trajectory, magnetic field lines threading Jupiter's diffuse aurora were initially sampled, transitioning to Zone-I from 13:38:15, then to Zone-II from 13:39:15 until 13:40:30, after which Juno was in the polar cap. The plasma wave spectra show significant wave power in both the E-fields and B-fields beginning as Juno entered Zone-I. Below f_{cH3+}, intense electromagnetic waves with a dispersive spectral character, that is, a frequency dependence with time, extends throughout Zone-I. This is followed by an intense broadband electromagnetic emission that extends throughout Zone-II. There are jumps in both the low-frequency electric and magnetic field spectral densities at the boundary between Zone-I and Zone-II suggesting the mode is not continuous across. There are intermittent bursts of broadband emissions mostly in Zone-II. Above f_{cH+} and from equatorward of Zone-I, an electromagnetic emission is present with a clear lower frequency cutoff that is continuous across and throughout Zone-I. This lower frequency cutoff decreases non-monotonically until Zone-I and extends well below f_{cH+}. Of particular interest is the lack of a clear whistler-mode auroral hiss signature which exhibits a funnel shape above f_{cH+} and is a key plasma wave feature of planetary auroral regions (also commonly known as VLF saucers) (e.g., Gurnett et al., 1983).

The magnetic field data show intense transverse fluctuations, interpreted as low-frequency Alfvén fluctuations, that extend throughout the region equatorward and stop short of Zone-I. There is likely some evidence of this fluctuation within Zone-I, albeit to a much lesser extent. However, this is near the low-frequency noise level and should be interpreted with care. The strongest field-aligned current, manifested as a large gradient in δB_φ perturbations in a narrow interval, marks the entry into Zone-I. Interestingly, this is clearly separated from the transverse fluctuations, which are largely equatorward of Zone-I. The δB_φ gradient is interpreted as an upward field-aligned current. In Zone-II, the gradient reverses, but falls off much more slowly, indicating downward field-aligned current region that is distributed over a larger region and is not as ordered and continuous as its Zone-I counterpart.
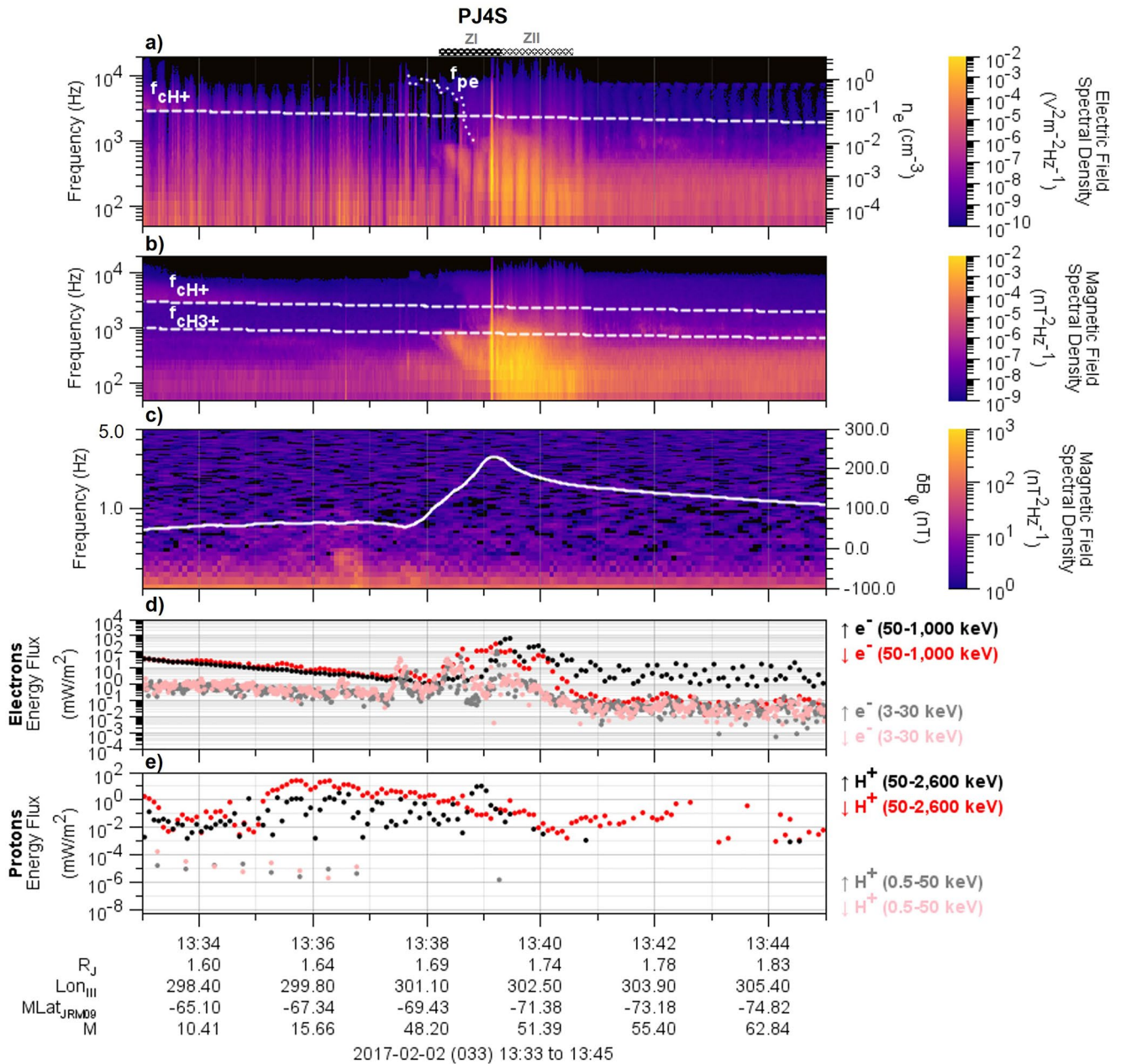
Figure 2. Plasma waves, magnetic field, and charged particles when Juno was magnetically connected to Jupiter's southern auroral zone near its fourth perijove (PJ4S). (a, b) Electric and magnetic field frequency-time spectrogram, respectively, measured by Waves. Overlaid onto each are the H^+ and H_3^+ cyclotron frequencies, f_{cH+} f_{cH3+}, as white dashed lines. The electron plasma frequency, f_{pe}, is digitized as the lower frequency cutoff of the Ordinary mode and shown as a white dotted line. The y-axis on the right converts f_{pe} in Hz to electron number density, n_e, in cm^{-3}. (c) Transverse magnetic field fluctuations measured by the magnetometer. Overlaid is the perturbation in the azimuthal magnetic field, δB_φ, as a white solid line. (d) Electron energy fluxes measured by Jovian Auroral Distributions Experiment (JADE) (light colors) and Jupiter Energetic-particle Detector Instrument (JEDI) (dark colors) over the energy ranges 3–30 keV and 50–1,000 keV, respectively. Black/gray and red/pink correspond to upward and downward populations, respectively. (e) Proton energy fluxes measured by JADE (light colors) and JEDI (dark colors) over the energy ranges 0.5–50 keV and 50–2,600 keV, respectively. Black/gray and red/pink correspond to upward and downward populations, respectively.

The electron energy flux shows bidirectional populations in both energy ranges equatorward of Zone-I and asymmetries emerge as Juno enters Zone-I. Just equatorward of the Zone-I boundary, there is a peak in the lower (3–30 keV) energy electron flux with more downward than upward fluxes. This is followed by a clear separation between the fluxes in the higher (50–1,000 keV) energy range in Zone-I with the downward energy fluxes dominating by up to ~100× compared to the upward energy fluxes. In Zone-II, the asymmetry in the higher-energy electrons is clearly reversed, with greater upward energy fluxes than downward, also by ~100×.

The data for H^+ energy fluxes are more limited in cadence compared to the electrons. In the higher (50–2,600 keV) energy population, there are episodes of bidirectionality, but the clearest feature is the dominant upward H^+ energy fluxes near 13:39 in Zone-I by ∼100× compared to the downward energy fluxes.

4. Detailed Analysis and Discussion

Various data sets have identified distinct features observed over Jupiter's main aurora (e.g., Allegrini et al., 2020; Gershman et al., 2019; Kotsiaros et al., 2019; Mauk et al., 2020; Szalay et al., 2017, 2021); however, these are yet to be analyzed altogether, and including a plasma wave analysis, to determine their association between the different zones and, more importantly, how they can be reconciled and fit into the bigger picture of Jupiter's auroral generation mechanisms.

In addition to Figure 2 (PJ4S), we include three more multi-instrument time series when Juno was magnetically connected to the auroral zones. These are shown in Figures 3–5 for PJ6S, PJ7N, and PJ9S, respectively. The format is the same as that of PJ4S, noting that PJ7N is a northern pass and Juno was moving equatorward from left to right. Given the similarities that will be discussed, we do not go through each figure in detail but will highlight certain unique features where necessary. We focus our analysis on Zone-I and Zone-II, which are thought to carry Birkeland currents.

4.1. Zone-I

Zone-I occurs at intermediate latitudes just poleward of the diffuse aurora. The exact latitudes depend on hemisphere and local time. This region is by far the narrowest in latitude among the auroral zones as shown in Figure 1, but its clearly defined equatorward and poleward boundaries, as well as the high repeatability among the various data sets, make it the most straightforward to identify. Mauk et al. (2020) characterized this region with dominant downward energetic electrons within the loss cone.

Kotsiaros et al. (2019) and Mauk et al. (2020) noted an agreement between the upward field-aligned current and predominantly downward energetic electrons for the PJ6S auroral pass (shown here in Figure 3), suggesting that Zone-I is associated with upward electric currents. Figures 2–5 corroborate this correspondence between the 50 and 1,000 keV downward electrons and the well-structured upward field-aligned current from δB_φ and confirm that most of the upward current is indeed carried by downward energetic electrons. It should be highlighted that although upward currents in Zone-I are well-ordered, the predominantly downward electron acceleration supporting these currents is via both inverted V and broadband distributions, often the latter attaining higher energies (Mauk et al., 2017b). These distributions have been observed serially within the same Zone-I pass and are occasionally overlaid onto one another (see figures 8 and 12 in Mauk et al. (2020)). While the domination of the downward energetic electron is a reliable predictor of Zone-I, there exists large variability in the size of the asymmetry between the downward and upward energy fluxes among the different events. This can be as large as 100× (e.g., PJ4S) and as relatively modest as 3–5× (e.g., PJ6S and PJ9S). The size of the asymmetry is likely related to both the nature of the acceleration region and Juno's proximity to it.

Kurth et al. (2018) showed for PJ7N that an interval of downward broadband electron distribution (in what was later identified as Zone-I) is coincident with brief but very intense broadband plasma waves in both the electric and magnetic spectra (∼01:15:51 in Figure 4). It appears that this correspondence is repeatable across events whenever broadband electron distributions are present, for example, at 13:39:07 during PJ4S in (Figure 2). There are, however, no plasma wave signatures that uniquely correspond to downward inverted V electron distributions. Kurth et al. (2018) proposed the importance of these intense broadband electromagnetic waves in intervals of broadband electron acceleration and determined the direction of their Poynting vector with respect to the Jovian magnetic field to show that they were propagating in the same direction as the predominantly downward energetic electrons. These waves were interpreted as being in the whistler mode as the frequency extended well above f_{cH+} and assumed to cut off at the electron plasma frequency, f_{pe}, at ∼10 kHz (or $n_e \approx 1.2$ cm^{-3}), which represents the theoretical upper-frequency cutoff for whistler-mode waves in the presence of a strong magnetic field (e.g., Persoon et al., 2019). We will show in the next section, however, that Zone-I is a region where the electron densities are dramatically depleted to as low as <0.01 cm^{-3}, or $f_{pe} < 900$ Hz. Densities could not be inferred *within* these brief intervals of broadband acceleration; therefore, the presence of the whistler mode would imply that the densities are anomalously greater during these intervals. Broadband electromagnetic waves
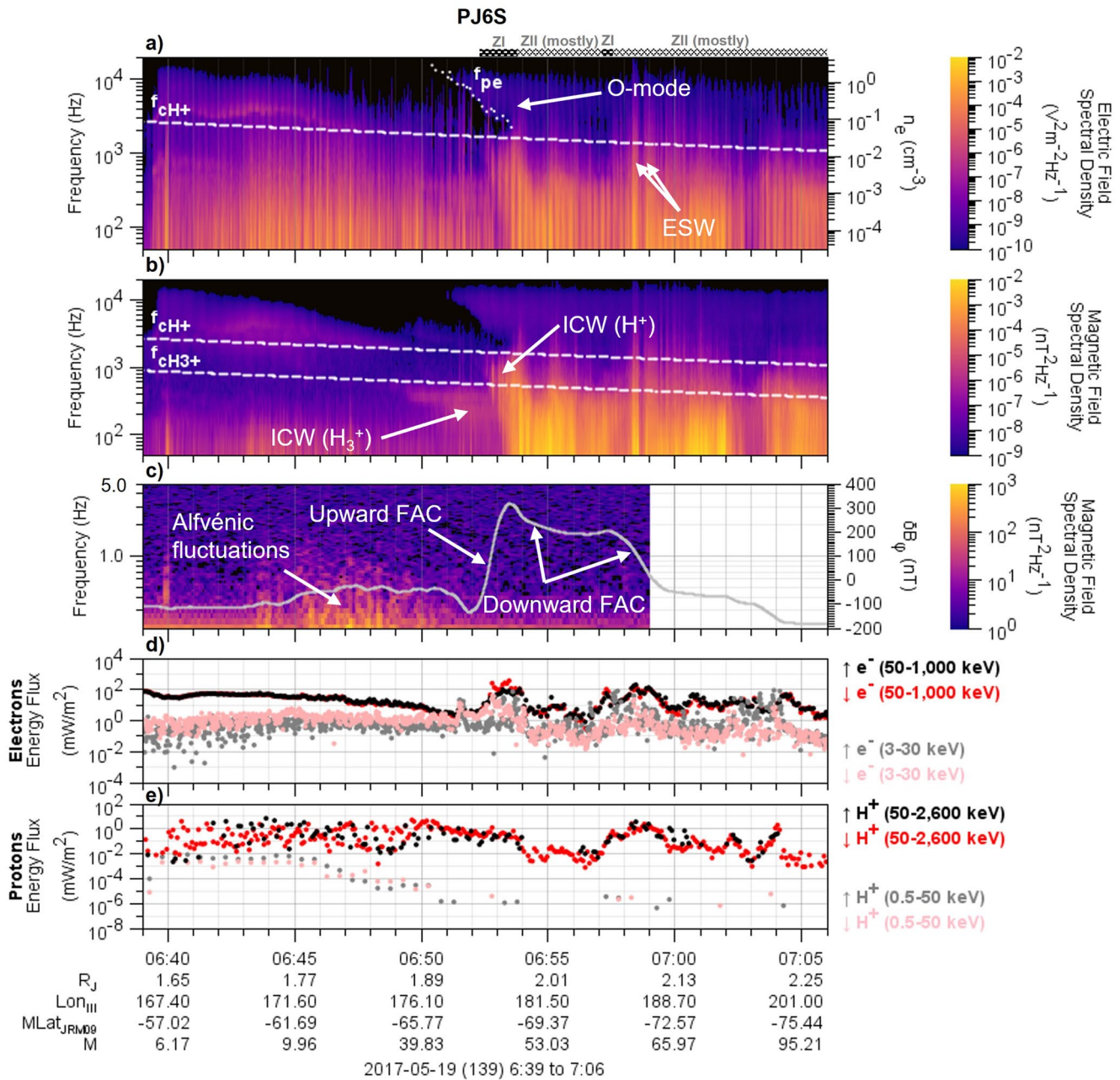
Figure 3. Same as Figure 2 but for Jupiter's southern auroral zone near its sixth perijove (PJ6S) and annotated.

are routinely observed over Earth's auroral regions, although typically confined to the downward current regions (Ergun et al., 1998b) and have also been reported in Jupiter's polar cap region (Elliot et al., 2020). We will revisit these features and show their correspondences against energy- and pitch-angle-time spectra when discussing Zone-II as they appear to be much more prevalent there.

Another important observation in Zone-I is the lack of, or significant reduction in, Alfvénic fluctuations compared to just equatorward in the diffuse aurora. Alfvén waves are known to develop parallel electric fields when finite electron mass is considered and their role has therefore been posited to explain the broadband nature of Jupiter's auroral electrons (Lysak et al., 2021; Saur et al., 2018). It is therefore likely that these waves have dissipated at higher Zone-I altitudes, lending most of their energy to electron acceleration. It is important to note that Jupiter's low-altitude region is characterized by very strong magnetic fields meaning any Alfvénic fluctuations present
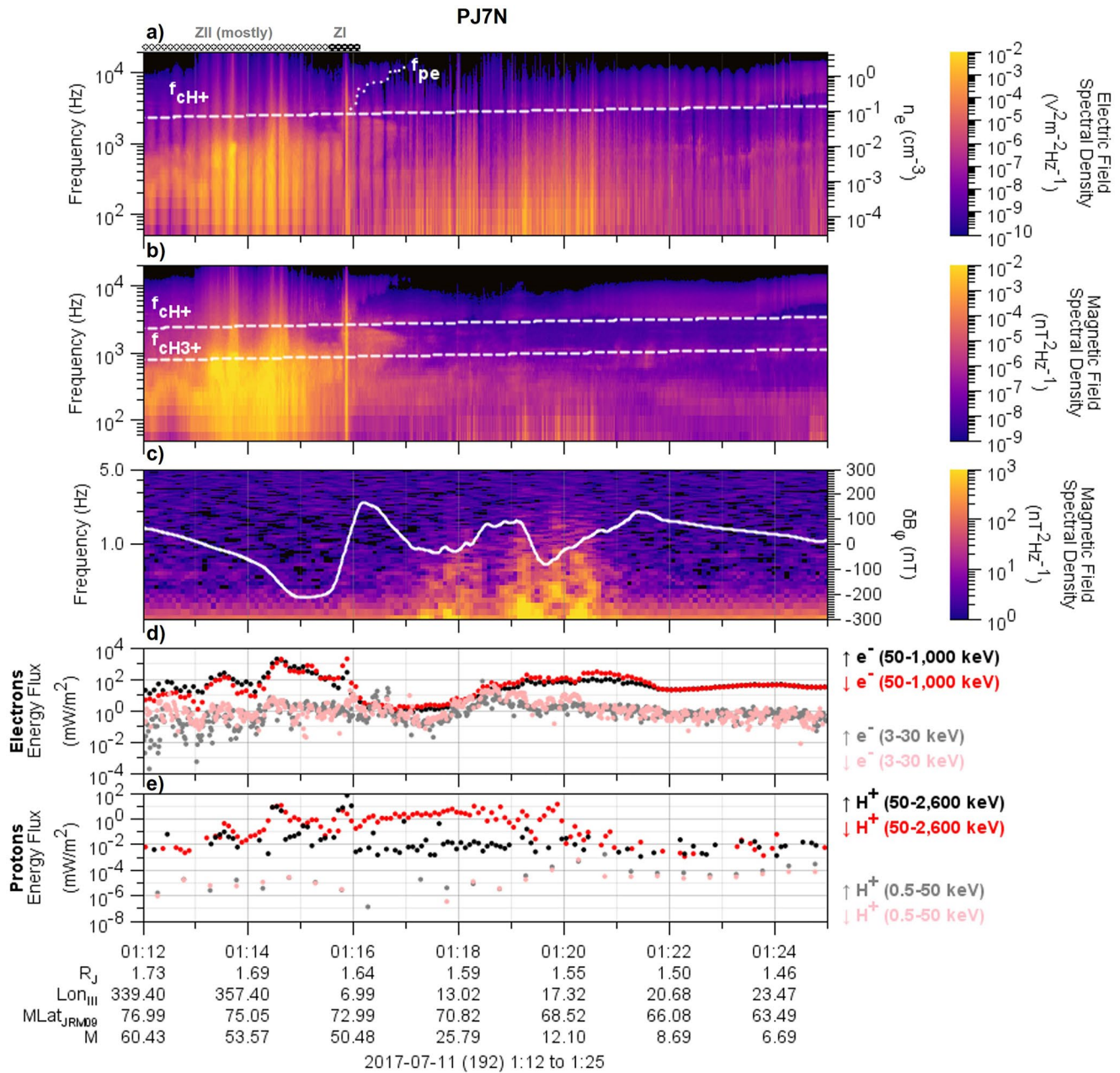
Figure 4. Same as Figure 2 but for Jupiter's northern auroral zone near its seventh perijove (PJ7N).

may just be too small to be picked up by the magnetometer. The Poynting flux is estimated as $\delta B^2 v_A/\mu_0$, where v_A is the Alfvén speed which considerably rises in the presence of significant density depletions. Therefore, for a given Poynting flux, it follows that δB would decrease correspondingly.

It is worth emphasizing that the Alfvénic fluctuations are repeatable signatures of the diffuse aurora, but not Zone-I or Zone-II. The waves are clearly supported over a wide range of M-shells. Allegrini et al. (2020) presented a survey showing that the lower-energy 3–30 keV electrons typically peak just equatorward of the main oval (or what is now called Zone-I). It appears from Figures 2–5 that the poleward edge of the Alfvénic fluctuations is when the 3–30 keV electrons peak and precedes the higher 50–1,000 keV that dominate Zone-I. Interestingly, during PJ4S and PJ7N (Figures 2 and 4), the Alfvénic fluctuations diminish in the diffuse aurora as the 3–30 keV electron energy fluxes peak at ~13:37:30 and ~1:18:30, respectively, before recovering again. Li et al. (2021) applied a data-model comparison to show that whistler-mode waves are the driver of Jupiter's diffuse
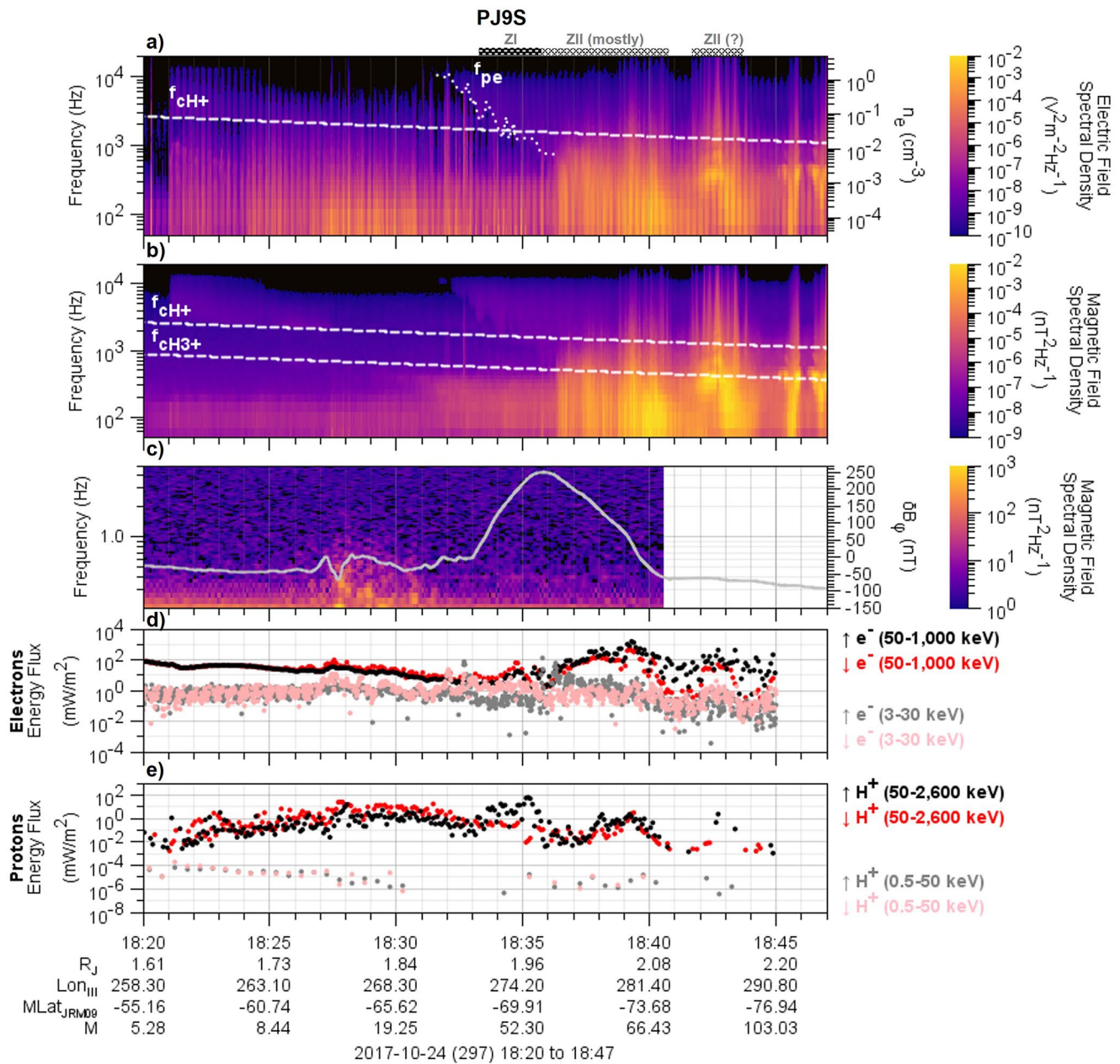
Figure 5. Same as Figure 2 but for Jupiter's southern auroral zone near its ninth perijove (PJ9S).

auroral precipitation above several keV via pitch-angle scattering, although this mechanism did not account for the observed precipitation of lower energies (< several keV) and was limited to lower latitudes (M-shells 8–18). Based on our observed correspondences, we postulate that Alfvén waves may indeed be responsible for precipitating lower energy electrons in the diffuse aurora at the higher latitudes.

The most prominent plasma wave signature in Zone-I are intense emissions below f_{cH+} and f_{cH3+}. The electric and magnetic field spectral densities are enhanced over a broad range of low frequencies (few kHz bandwidths) and undergo a distinct drop in intensity at f_{cH+} and/or at f_{cH3+}. This is usually an indication of strong damping via cyclotron resonance where the wave energy is transferred to the corresponding ions. This characteristic is consistent with ion cyclotron waves and their observation in the presence of upward energetic ions and downward energetic electron beams draw a strong analogy to both Earth's and Saturn's upward current regions where the correlation has been observed (e.g., Bader et al., 2020; Cattell et al., 1988; McFadden et al., 1998; Mitchell

et al., 2009). Ion cyclotron waves in the auroral regions have been observed as both electrostatic (EIC) and electromagnetic (EMIC) modes. The strong magnetic component here is evidence that EMIC waves are present, though not necessarily in the absence of EIC, and the significance is that they carry Poynting fluxes.

Figures 6a–6d show an analysis of the Poynting vector direction for these waves during PJ4S. These are the emissions present below 1 kHz and the series of peaks and nulls in the electric field spectrum is due to spin modulations. The electric and magnetic field fluctuations have high coherency, $C_{Ey\text{-}Bz} \approx 1$, and the combination of a phase $\varphi_{Ey\text{-}Bz} \approx -180°$ (or 180°) and a positive $B_x/|B_x|$ in the southern hemisphere indicates an upward-propagating wave. Figure 6e shows that the power of these waves primarily resides perpendicular to the magnetic field. Here we compare the spin-modulations in the electric field spectral densities to the angle between the antenna dipole and background magnetic field and show that spectral densities peak (depress) when the antenna is perpendicular (parallel) to the magnetic field. At the measured frequency of $\frac{1}{4} f_{cH+}$, the ratio of the components is $E_\perp/E_\parallel = 200$. Despite a strong magnetic component, the E/cB ratio (not shown here) is greater than one but of order unity. This can occur in the presence of an admixture of EIC and EMIC waves.

Although we cannot directly verify that they are intrinsically left-hand-polarized, we can indirectly infer this from the fact that their electric and magnetic fields are highly coherent, fluctuate perpendicular to the background magnetic field, and do not propagate above f_{cH+} or f_{cH3+}. Altogether, these are consistent with resonant absorption of left-hand-polarized ion cyclotron waves, a well-recognized mechanism for ion heating (e.g., André et al., 1998; Chang et al., 1986; Lysak, 1986). The observed (mostly) upward-propagation of these waves is somewhat in contrast to what is typically observed during low-altitude passes of Earth's aurora, where waves below f_{cH+} are more commonly observed to be downward propagating (Chaston et al., 1998; Gurnett et al., 1984). The difference at Jupiter may be either due to their sources originating at an altitude lower than Juno, that is, $\lesssim 1\ R_J$ above the one-bar level, or a different generation mechanism altogether. Electron drifts as the source of free energy driving ion cyclotron instability have been invoked to explain their correlation with auroral field-aligned currents (Cattell et al., 1998). Testing whether this hypothesis holds at Jupiter requires solving dispersion relations with modeled particle distributions which is beyond the scope of this study. It has been further demonstrated that broadband EMIC waves can also accelerate cold secondary electrons to form counterstreaming field-aligned electrons (McFadden et al., 1998). Since bidirectional electrons are a key feature of Jupiter's auroral zones, the role of EMIC waves should not be neglected.

The coincident field-aligned H^+ fluxes suggest that any perpendicular heating by the ion cyclotron waves is not sufficient to deviate the pitch angle from the field-aligned direction and generate conics. The measured electric field spectral density of 10^{-5} V m^{-1} Hz^{-1} near f_{cH+} (Figure 6e) yields a maximum cyclotron resonant heating rate of ~500 eV/s (Chang et al., 1986) and is comparable to that measured in Io's Main Alfvén Wing where, by contrast, H^+ conics were detected (Clark et al., 2020; Sulaiman et al., 2020). The difference is likely due to the interaction time, proximity to, nature of the acceleration region or a combination thereof. Szalay et al. (2021) concluded, based on the presence of H^+ inverted V distributions, that quasi-static parallel potential structures drove the acceleration of H^+ away from Jupiter's high-latitude ionosphere. This is further supported by the disappearance of upward H^+ during intervals of broadband acceleration within Zone-I shown by Mauk et al. (2018). The observation of both downward electron and upward H^+ beams at these altitudes would suggest that Juno was in or close to a unidirectional acceleration region, that is, an upward parallel potential. Therefore, it is possible that the perpendicular heating supplied by ion cyclotron waves is overcome by the action of more powerful parallel potentials that deposit much larger amounts of energy along the field line. The ion cyclotron waves (shown to be upward propagating) may have their source in the ionosphere where the density is high and enough ions exist to significantly dampen the waves. Cold ionospheric ions are bound by Jupiter's large gravitational potential (the gravitation binding energy of H^+ is ~20 eV and H_3^+ is ~60 eV) and to be admitted into the electrostatic potential at higher altitudes, a means of energization is required to escape the gravitational potential. When ions are heated perpendicular to the magnetic field in the presence of a diverging magnetic field, they experience a mirror force that transports them to a region of weaker magnetic field, that is, higher altitudes, as a parallel velocity component develops to conserve kinetic energy and the first adiabatic invariant.

In summary, a multi-instrument *in-situ* analysis shows that the following criteria identify Zone-I in Jupiter's low-altitude auroral region: (a) presence of a gradient in the B_φ perturbation that is indicative of an upward field-aligned current, as measured by MAG; (b) greater downward electron energy fluxes than upward, as well as greater than outside the loss cone, accompanied by broadband and/or inverted V distributions as measured by
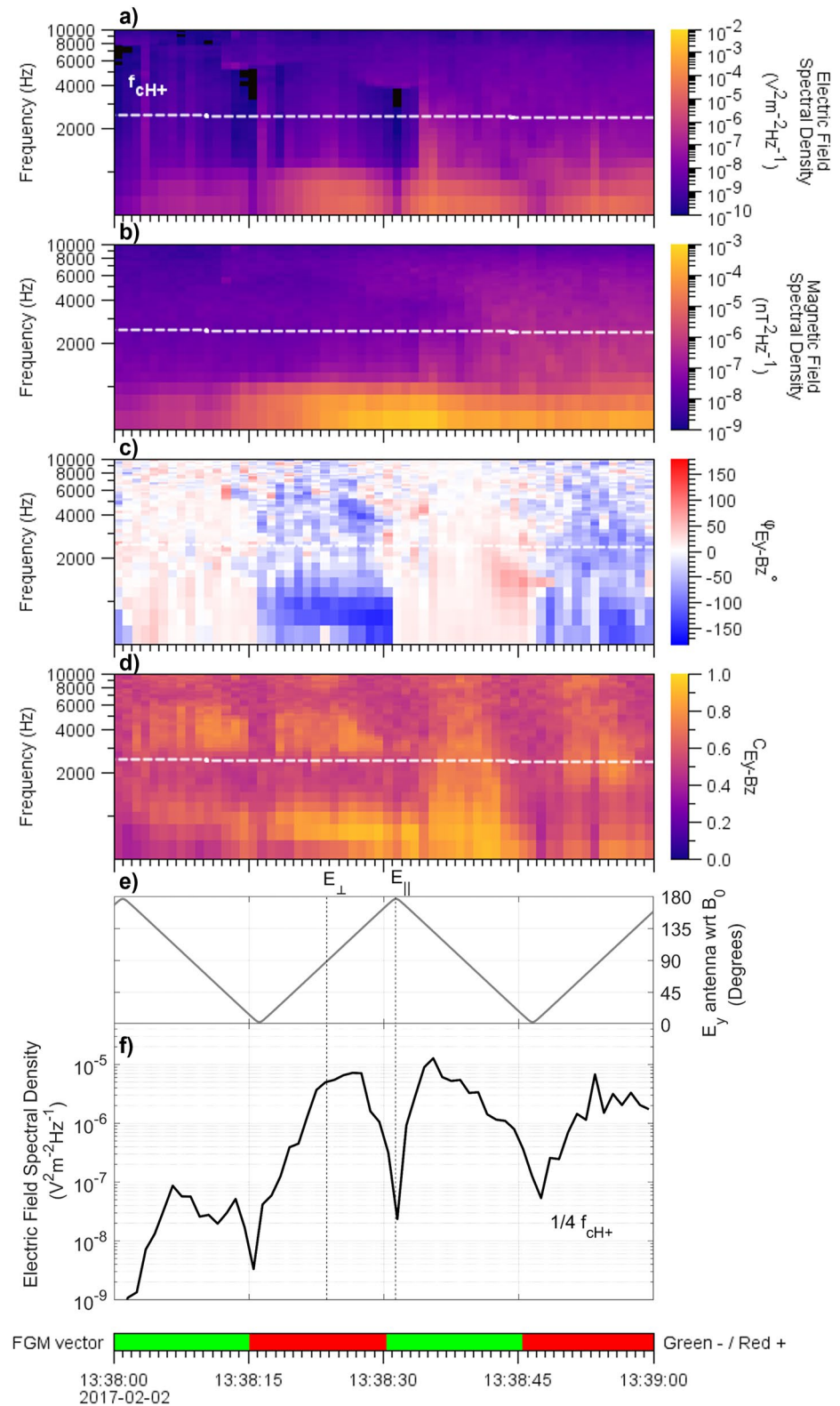
Figure 6. Poynting vector analysis during PJ4S. (a, b) Electric and magnetic field frequency time spectrograms, respectively. (c, d) Phase difference and coherence between measured electric and magnetic fields, respectively. (e, f) Angle between electric field antenna and background magnetic field correlated against the electric field spectral density at ¼ f_{cH+}.
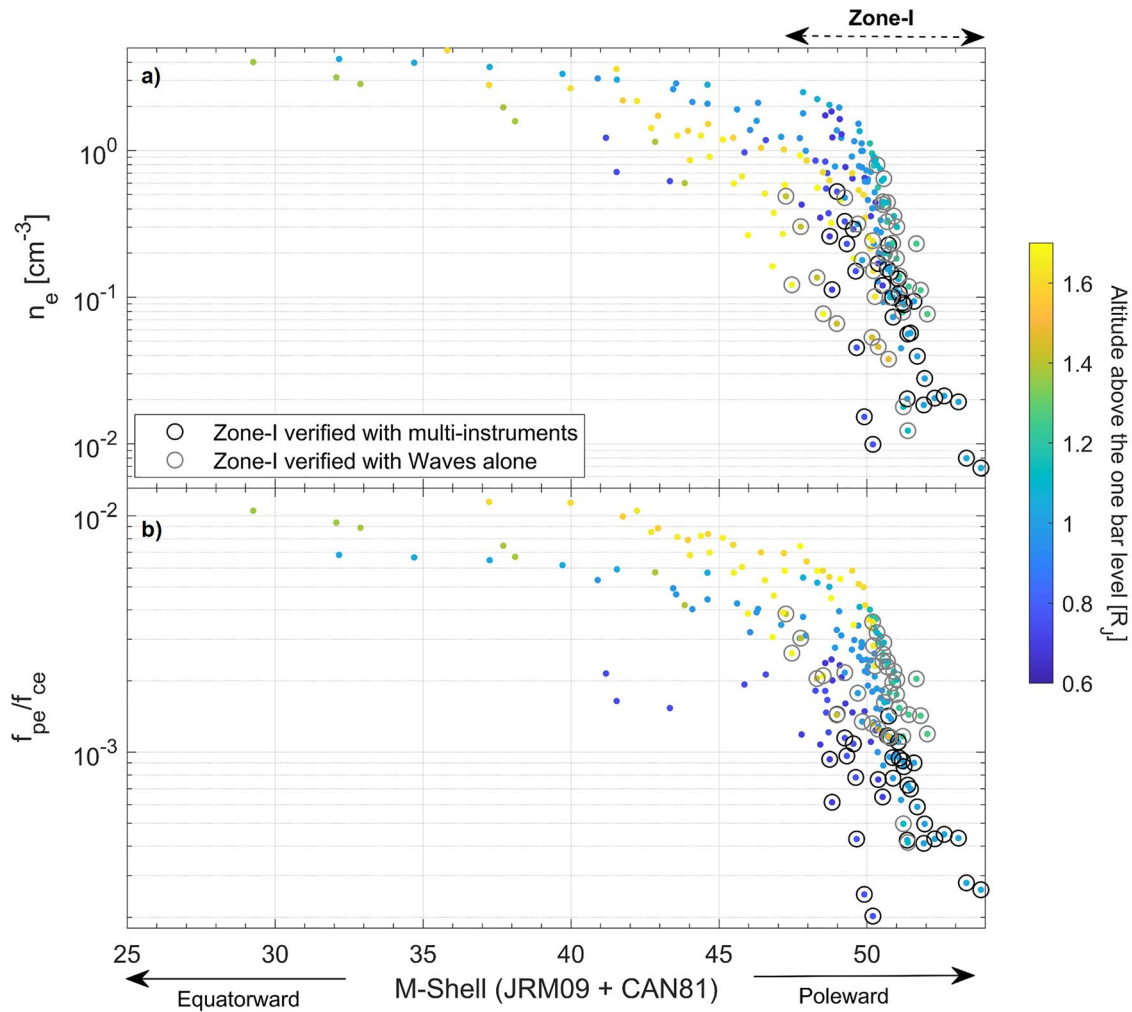
Figure 7. (a) Electron number density plotted against M-shell and color-coded with Juno's altitude above Jupiter's one-bar level. The circled data points are when Juno was magnetically connected to Zone-I. (b) f_{pe}/f_{ce} plotted against M-shell, same format as (a). The M-shell was calculated using the JRM09 internal field model (Connerney et al., 2018) + an external current sheet model (Connerney et al., 1981). This is likely overestimating the true M-shell.

JEDI; (c) the low-frequency portion of intense, apparently dispersive, coherent, mostly upward-propagating ion (H^+ and/or H_3^+) cyclotron waves, as measured by Waves; and (d) presence of field-aligned upward flowing H^+, as measured by JADE and JEDI. These observations are unique to Zone-I and highly repeatable, such that any one of them is highly predictive of Zone-I. Furthermore, they exhibit distinct and unambiguous equatorward and poleward edges that are consistent with the main oval emission shown in Figure 1. The boundary at which Alfvénic fluctuations significantly decrease reliably marks the entry into Zone-I from the diffuse aurora. The deficiency in observed Alfvénic fluctuations, however, is not a unique marker of Zone-I as this is continuous into Zone-II.

4.2. Electron Density Depletions in Zone-I

Electron density depletions occur within Zone-I, exhibiting large variability and with an equatorward edge. The scatter plot in Figure 7a shows the electron number density variation with increasing M-shell. This is color-coded in altitude over a range of 0.6–1.7 R_J above the one-bar level. The direction of increasing M-shell translates into Juno sampling the auroral regions in the poleward sense, beginning with the equatorward edge of the broad

diffuse aurora through to the poleward edge of Zone-I. The M-shells here are likely overestimated since the auroral regions are believed to be mapped to ~30 R_J in the equatorial plane. The purpose of this figure is to examine how the electron densities vary on different auroral field lines. It should be noted that different internal field and/or current sheet models will yield different M-shell values. We therefore identify the auroral crossings based on in-situ observations and do not rely on the values provided by M-shell mapping.

We digitize the densities by identifying Ordinary (O) mode waves that are sometimes present during the auroral passes. The O-mode is a transverse electromagnetic wave. Its dispersion relation is one of two derived from the cold-plasma approximation for propagation perpendicular to the **B**—the other being the extraordinary (X) mode more familiarly recognized as radio waves. The main difference is the relatively simpler dispersion relation of the O-mode which is the same as that for an unmagnetized plasma. The waves are evanescent below f_{pe} and therefore exhibit a low-frequency cutoff, as shown in the first panels of Figures 2–5 (see Sulaiman et al. (2021) for the theoretical background as well as early and more recent implementations of this technique by Gurnett and Shaw (1973) and Elliott et al. (2021)). Strictly speaking, this cutoff is an upper limit to the local electron plasma frequency due to the possibility of a higher-density region existing between the source and the spacecraft. When this occurs, the measured cutoff corresponds to the maximum density between the source and the spacecraft; however, the cutoffs observed here are usually well-defined and continuous which suggest the densities are local. Since $f_{pe} \propto \sqrt{n_e}$, the total electron number density is straightforwardly obtained and this is in excellent agreement with the electron partial density derived by JADE for overlapping intervals (see Figure S2 in Supporting Information S1—the electron partial densities derived by JADE were mostly limited to the diffuse aurora; Allegrini et al., 2021). Despite the limited coverage in altitude shown here, the expected anti-correlation between density and altitude is present, giving confidence in our method. We obtain density measurements whenever the O-mode waves are present and discernible. The circled points highlight measurements taken when Juno was magnetically connected to Zone-I using all the criteria whenever the O-mode was present during the first 10 perijoves. When the pitch angle coverage was suboptimal, only criterion (c) was used. Recall that any one of the criteria alone is a sufficient marker of Zone-I.

Figure 7a exposes a boundary between the diffuse aurora and Zone-I. Within Zone-I, the electron densities are, on average, significantly depleted, by up to 2 orders of magnitude down to below 0.01 cm^{-3}. In Zone-II, the sub-f_{cH+} band of the O-mode waves becomes "washed out" in the spectrogram due to the presence of intense broadband low-frequency electromagnetic emissions; therefore, it is not possible to determine, based on this technique, how far they remain depleted and whether/where they recover. All Zone-I verified densities are below 0.1 cm^{-3} with a subset below 0.01 cm^{-3}.

Density depletions, or auroral cavities, are known to be intimately related to auroral acceleration processes (e.g., Paschmann et al., 2003; Persoon et al., 1988). Their association is well supported by theoretical modeling (Block & Fälthammar, 1968; Knight, 1973) and repeatedly corroborated by experimental evidence (Ergun et al., 2002; Hull et al., 2003) although much of the focus has been on the development of parallel potentials in the context of inverted V distributions. The basic principle is that density depletions reduce the number of charge carriers thereby limiting the ability of plasmas to carry strong field-aligned currents. This "current choke" results in the development of parallel electric fields as the displacement current term of Ampère's law builds up to ensure $\nabla \times \mathbf{B}$ is balanced (Ray et al., 2009; Song & Lysak, 2006).

Although turbulence-induced broadband processes are typically associated with weaker Alfvénic aurora at Earth, they are believed to be of greater importance than electrostatic acceleration processes in generating Jupiter's most intense aurora (Clark et al., 2018; Saur et al., 2018). Parallel electric fields from Alfvén waves become important when the $k_\perp^2 \lambda_e^2$ term is large, where λ_e is the electron inertial length given by $c/2\pi f_{pe}$ and $k_\perp$ is the wave vector component perpendicular to the background magnetic field. A large $k_\perp$ can be satisfied by a converging flux tube as the area is inversely proportional to B. A low-density region, or greater λ_e, means Alfvén waves undergoing a turbulent cascade are dissipated "earlier" in k-space. The measured densities in Zone-I equate to λ_e as large as 50 km, larger than 20–30 km modeled by Saur et al. (2018), thereby further lowering the threshold for Alfvénic dissipation to be achieved in the high-latitude region. Dispersive Alfvén waves have been observed within deep density cavities over Earth's auroral oval together with upgoing transversely heated ionospheric ions and downgoing field-aligned electrons. This has been interpreted as evidence for a positive feedback mechanism, whereby

small-scale Alfvén waves erode the auroral ionosphere by facilitating ion outflow, which in turn leads to deeper density cavities that maintain the production of small-scale Alfvén waves via refraction and phase mixing of incoming large-scale Alfvén waves (Chaston et al., 2008; Rankin et al., 1999). More recently, Lysak et al. (2021) proposed that an ionospheric Alfvénic resonator (IAR) operating at Jupiter can account for the observed broadband electron distributions. This is a widely accepted model used to explain similar distributions in the case of Earth, whereby the propagation of Alfvén waves is facilitated by a rapid decrease in density (Lysak, 1991). The corresponding increase in Alfvén speed gives rise to partial reflection of Alfvén waves which become trapped. At large enough $k_\perp$, the parallel electric field fluctuating at some resonant frequency can result in electron acceleration over a broad range of energies.

Figure 7b combines the electron densities with measured magnetic field strengths to express f_{pe}/f_{ce} variations. This ratio is especially important for the generation of radio emissions via the Cyclotron Maser Instability (Wu & Lee, 1979). This mechanism requires $f_{pe}/f_{ce} \ll 1$ in the presence of a positive gradient in the perpendicular velocity distribution of weakly relativistic electrons. It is clear that the necessary low f_{pe}/f_{ce} is well satisfied, particularly in Zone-I, thus will provide further constraints on Jupiter's radio sources (e.g., Imai et al., 2019; Louis et al., 2019).

4.3. Zone-II

Among the three zones, Zone-II occurs at the highest latitudes just poleward of Zone-I. This region has a clearly defined equatorward boundary, but its poleward boundary with the polar cap is often ambiguous. Mauk et al. (2020) characterized this region with upward energetic electrons with energy fluxes greater than or equal to the downward component within the loss cone. Another key difference is the bidirectional electrons are almost always broadband in energy. On the other hand, downward H^+ inverted Vs have been observed intermittently and, by contrast to Zone-I's highly field-aligned H^+ beams, exhibit a nearly isotropic pitch angle distribution with an empty upward loss cone (Mauk et al., 2020). Whereas Zone-I features are typically (but not always) continuous within its boundaries, Zone-II features are spatially or temporally sporadic.

Kotsiaros et al. (2019) and Mauk et al. (2020) noted agreements between the downward field-aligned currents and Zone-II during the PJ6S auroral pass (Figure 3), although this is usually limited to the most intense portion of the energetic particles and not as simple as the more ordered Zone-I. Again, Figures 2–5 corroborate this correspondence. Observed Alfvénic fluctuations in Zone-II remain relatively low/absent and comparable to Zone-I. This could also be evidence of dissipation, especially in a region supported predominantly by broadband, bidirectional energetic electrons (Lysak et al., 2021; Saur et al., 2018) and in the absence of strong evidence for inverted Vs and thus local parallel potentials. The plasma wave emissions, on the other hand, are the most intense of all zones with the largest average amplitudes in both the electric and magnetic fields. These are present throughout Zone-II and majority of the power is confined to frequencies below f_{cH+} (Figures 2–5), and are often accompanied by brief, intense emissions that extend well above f_{cH+} that resemble those sometimes observed in Zone-I. The difference is that these brief and intense emissions occur intermittently in Zone-I, whereas they appear to be a key feature of Zone-II and are correlated with the intervals of most intense energetic electrons which are in turn correlated with downward currents.

The downward current region is fundamentally different from its upward counterpart. The charge carriers are abundantly sourced from the cold, dense ionosphere as electrons and are accelerated by many orders of magnitude above their thermal energy. What is peculiar about Jupiter's Zone-II is that although the downward electron energy fluxes are generally no greater than the upward energy fluxes, they can be as intense or greater than the downward energy fluxes in Zone-I and sufficient to produce observable auroras (Mauk et al., 2020; and see Figure 1 here), in contrast to the "black aurora" at Earth and Saturn that are connected to flux tubes carrying downward currents. It is clear based on the difference in fields and particles characteristics that the acceleration mechanism in Zone-II is distinct and more observationally complicated than that supporting Zone-I. While Juno does not carry a DC electric field instrument, the various characteristics highlighted in the previous section support the sporadic presence (although not exclusively) of parallel potential structures in Zone-I. Other than the downward H^+ inverted Vs that are sometimes observed in Zone-II and not least that they are quasi-isotropic, the evidence for a stable parallel potential is inconclusive. The bidirectional electrons might be interpreted as

originating from potential structures above and below the spacecraft, however, this is not consistent with their broadband energy.

We emphasized in the previous section that EMIC waves should not be neglected in the context of electrons since their link has been established (McFadden et al., 1998), whereby cold secondary electrons are trapped and accelerated to form counterstreaming populations. It is therefore probably not a coincidence that the most intense waves below f_{cH+} occur in Zone-II, where bidirectional electrons are present.

An important piece of the puzzle for broadband electrons may be in the contemporaneous broadband emissions in the frequency-time spectrograms shown in Figures 8 and 9. In the frequency domain, large-amplitude solitary (or "spiky") structures in the waveform typically manifest as broadband noise. In other words, their steepness results in a broad range of frequencies displayed in the frequency domain; however, the underlying physics is in the waveforms. It is clear in Figures 8 and 9 that where broadband plasma wave emissions are seen, there are large-amplitude, spiky, and nonlinear electric field structures. Electrostatic solitary waves (ESWs) have been proposed to play a key role in accelerating electrons by carrying substantial potentials and are most often observed in Earth's downward current regions and in the presence of density depletions (Ergun et al., 1998b; Temerin et al., 1982). The ubiquity of these broadband emissions in Zone-II might be explained by the highly nonlinear evolution of two-stream electron beam instabilities, set up by bidirectional populations, that give rise to sharp pulses in the electric field (Matsumoto et al., 1994), as shown in Figures 8 and 9. Field-aligned electrons are then accelerated to a broad range of energies by the sum of individual micro-potential drops as they travel through ESWs. Despite their electrostatic nature, it is possible to measure an associated magnetic component (not shown here) which would result from the Lorentz field of a traveling charge.

Although the electron densities cannot be inferred within Zone-II, we can say with reasonable confidence that they remain low. The O-mode emissions above f_{cH+} appear continuous well into Zone-II with its low-frequency edge in the region below f_{cH+} that is dominated by intense electromagnetic turbulence. We therefore set f_{cH+} to be the approximate upper limit of f_{pe} and conclude that the electron densities within Zone-II are <0.1–0.01 cm^{-3}. Therefore, the correspondingly large electron inertial lengths in Zone-II would similarly lower the threshold for Alfvénic dissipation, which remains the leading mechanism to account for the observed electron spectra (Lysak et al., 2021; Saur et al., 2018). Whether the densities are comparable to Zone-I, of similar variability and/or spatial scales are important questions that are beyond the reach of our present density digitization methods.

Perhaps the most recognizable and commonly observed plasma wave feature above auroral regions is the whistler-mode auroral hiss. In a frequency-time spectrogram, they are easily identified by their characteristic funnel or V-shape (Gurnett, 1966; James, 1976) which arises when the wave normal angle approaches the whistler-mode resonance cone (Santolík & Gurnett, 2002). The favored generation mechanism is a coherent beam-plasma instability at the Landau velocity (Farrell et al., 1989; Maggs, 1989), that is, $\omega/k_\parallel \approx v_\parallel$. Since the auroral regions, including satellite auroral flux tubes, are a site for electron beams, whistler-mode auroral hiss are often observed and are often a reliable diagnostic for field-aligned currents (Gurnett et al., 1983, 2011; Sulaiman et al., 2018, 2020). That said, these plasma wave features are not as clearly identifiable in Jupiter's low-altitude auroral zones, contrary to expectation.

Figure 10 shows a rare example when the funnel-shaped auroral hiss was observed in the southern auroral zone during PJ12S. Although it appears like there are two similar emissions above and below f_{cH+}, they are fundamentally different and not connected since, above f_{cH+}, the timescales fall below the ion gyroperiod and the ions are effectively unmagnetized. The emission below f_{cH+} is the H$^+$ cyclotron mode commonly observed in Zone-I, likely propagating along its resonance cone. On the other hand, the emission above f_{cH+} is the whistler-mode auroral hiss, propagating along its own resonance cone. Auroral hiss is typically not seen to propagate down to as low as f_{cH+}. Along its resonance cone, the lower hybrid frequency, f_{LH}, represents a lower limit through which they cannot propagate but instead reflect off. In this highly magnetized regime, that is, $f_{ce} \gg f_{pe}$, we find $f_{LH} \simeq f_{cH+}$ (Sulaiman et al., 2021) and therefore conclude the waves are reflecting at the f_{cH+} boundary. While the whistler mode is typically observed as electromagnetic, its propagation along the resonance cone is quasi-electrostatic and this is supported by the relatively weaker magnetic component and an E/cB ratio of ~10. This mode is characterized by an index of refraction that is much greater than unity, that is, a phase velocity that is low. Therefore, the Landau
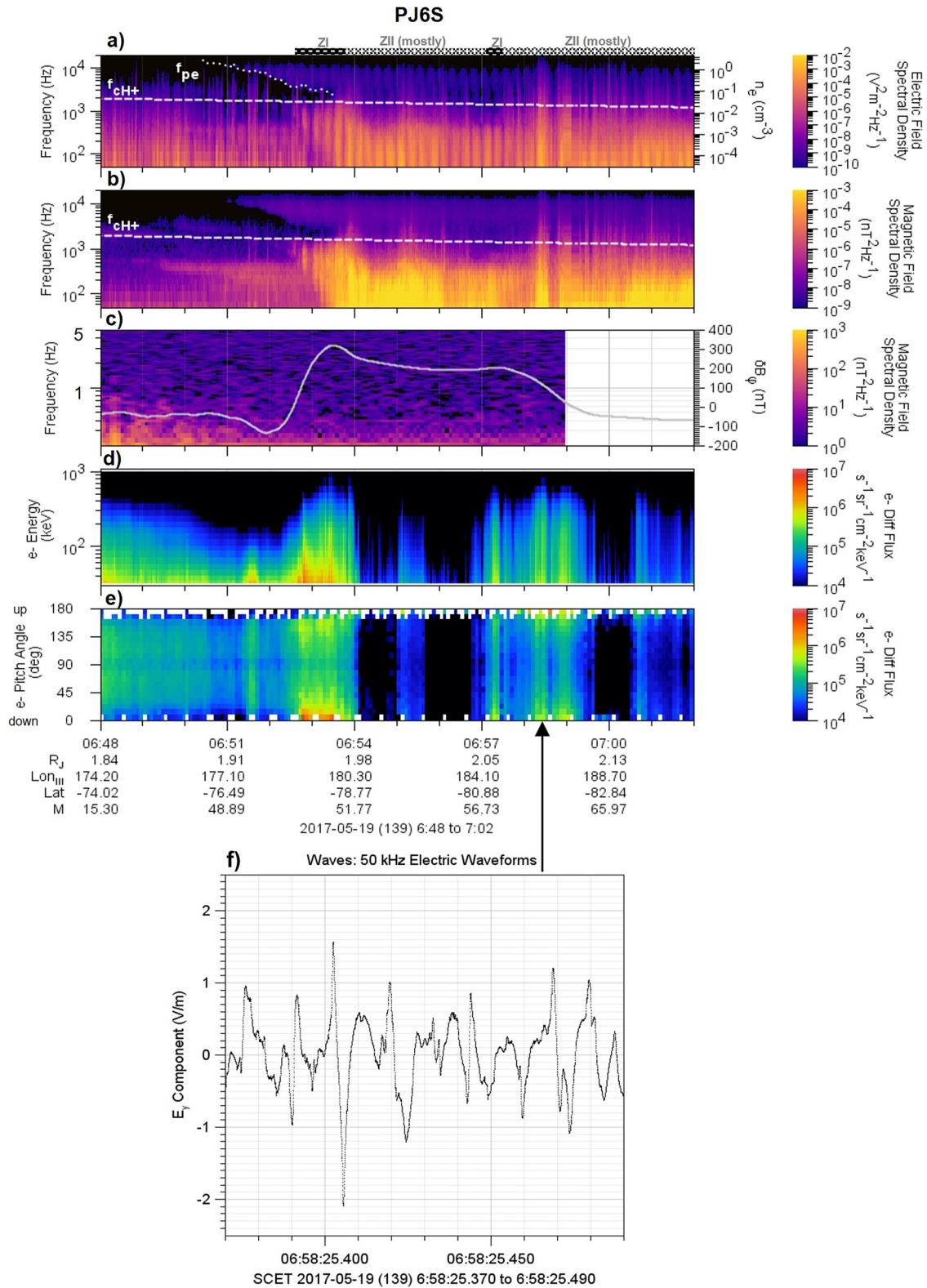
Figure 8.

resonance condition requires low-energy electrons for the beam-plasma instability. Higher-energy electrons that interact with higher phase velocities can generate electromagnetic waves that cease to exhibit the characteristic funnel shape. And even higher energies that exceed the maximum phase speed allowed by the dispersion relation will result in no Landau resonance altogether. This likely explains why quasi-electrostatic auroral hiss is not as common a feature at Jupiter's low-altitude region as at Earth owing to the much higher electron energies at play.

Finally, what has not been covered in this study are the properties of heavy ions. The clear cutoff of plasma waves in Zone-I at f_{cH3+} is indicative of H_3^+ cyclotron waves and is strong (indirect) evidence for presence of upward H_3^+. However, H_3^+ ions in the auroral zones have not been reported by the particle instruments at the time of writing. The presence of multiple heavy ions would have a significant impact since each additional ion introduces five characteristic frequencies: the standard cyclotron and plasma frequencies plus the more complex ion hybrid, multi-ion cutoff, and crossover frequencies, which require numerical solving. The latter three are highly sensitive to the fractional abundance of ions, let alone any individual density. This also means that composition can be constrained by modeling and correctly diagnosing wave modes and their characteristic frequencies. The significance of an ion hybrid frequency in a multicomponent plasma is that it modifies the wave mode's dispersion relation and therefore how it propagates through the medium. For example, a resonance cone can develop above each hybrid frequency (Santolík et al., 2016). The crossover frequency is that which the waves reverse their intrinsic polarization (left to right or vice versa) and can therefore affect the nature of wave-particle interactions.

5. Summary and Conclusions

We have provided a multi-instrument analysis on Jupiter's low-altitude Zone-I and Zone-II. Figure 11 is a graphical listing of the various observables identified in Zone-I and Zone-II, as well as the diffuse aurora, with the caveat that these structures are likely more complex and may exhibit considerable spatial and/or temporal variability, for example, during transient episodes like dawn storms (Bonfond et al., 2021; Ebert et al., 2021). As the spacecraft migrates to afford coverage of the low-altitude dawn aurora, spatial variability of the fields, particles, and plasma wave features will likely arise.

Our main conclusions are:

1. Zone-I and Zone-II are corroborated to be associated with upward and downward current regions, respectively.
2. Alfvénic fluctuations are most profoundly observed in the diffuse aurora and not in Zone-I and Zone-II. In the diffuse aurora, they intermittently diminish where 3–30 keV electron energy fluxes peak and are mostly absent in Zone-I and Zone-II, where 50–1,000 keV electron energy fluxes dominate. We suggest that this pattern is consistent with Alfvénic dissipation at higher altitudes.
3. The features of Zone-I are typically coherent across all fields, particles, and plasma wave observations. The equatorward and poleward boundaries are well defined.
4. The features of Zone-II are typically sporadic across all observables. The equatorward edge (with Zone-I) is well defined but the poleward edge with the polar cap can often be ambiguous.
5. The most prominent plasma wave modes are below the H^+ and H_3^+ cyclotron frequencies, f_{cH+} and f_{cH3+}. EMIC waves, and possibly including EIC waves, are commonly observed in Zone-I and in the presence of H^+ beams. They are typically upward propagating and fluctuate perpendicular to the magnetic field. We interpret them as the means by which gravitationally bound H^+ and H_3^+ can be energized and admitted into a parallel potential at higher altitudes.

Figure 8. Plasma waves, fields, and charged particles when Juno was magnetically connected to Jupiter's southern auroral zone near its sixth perijove (PJ6S). (a) Electric and (b) magnetic field frequency-time spectrogram measured by Waves. Overlaid onto each is the proton cyclotron frequency, f_{cH+}, as white dashed lines. The electron plasma frequency, f_{pe}, is digitized as the lower frequency cutoff of the Ordinary mode and shown as a white dotted line. The y-axis on the right converts f_{pe} in Hz to electron number density, n_e, in cm^{-3}. (c) Transverse magnetic field fluctuations measured by magnetometer. Overlaid is the perturbation in the azimuthal magnetic field, δB_φ, as a white solid line. (d) 50–1,000 keV electron energy-time and (e) pitch-angle-time spectrograms measured by Jupiter Energetic-particle Detector Instrument. The depletion near 90° is likely due to spacecraft shadowing and therefore not real. (f) Electric field waveforms corresponding to the time indicated by black arrows in stack plots.
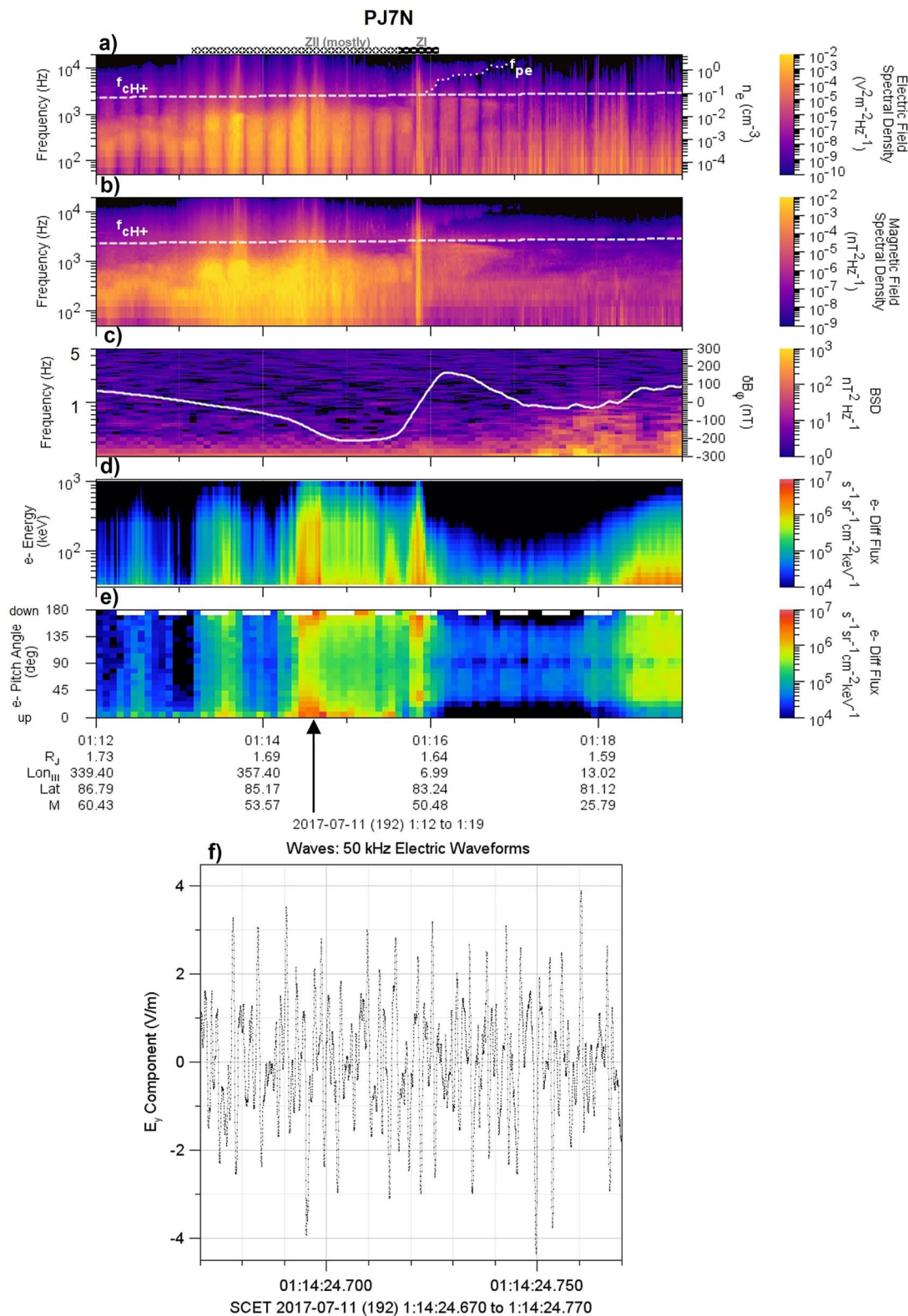
Figure 9. Same as Figure 8 but for Jupiter's northern auroral zone near Juno's seventh perijove (PJ7N).
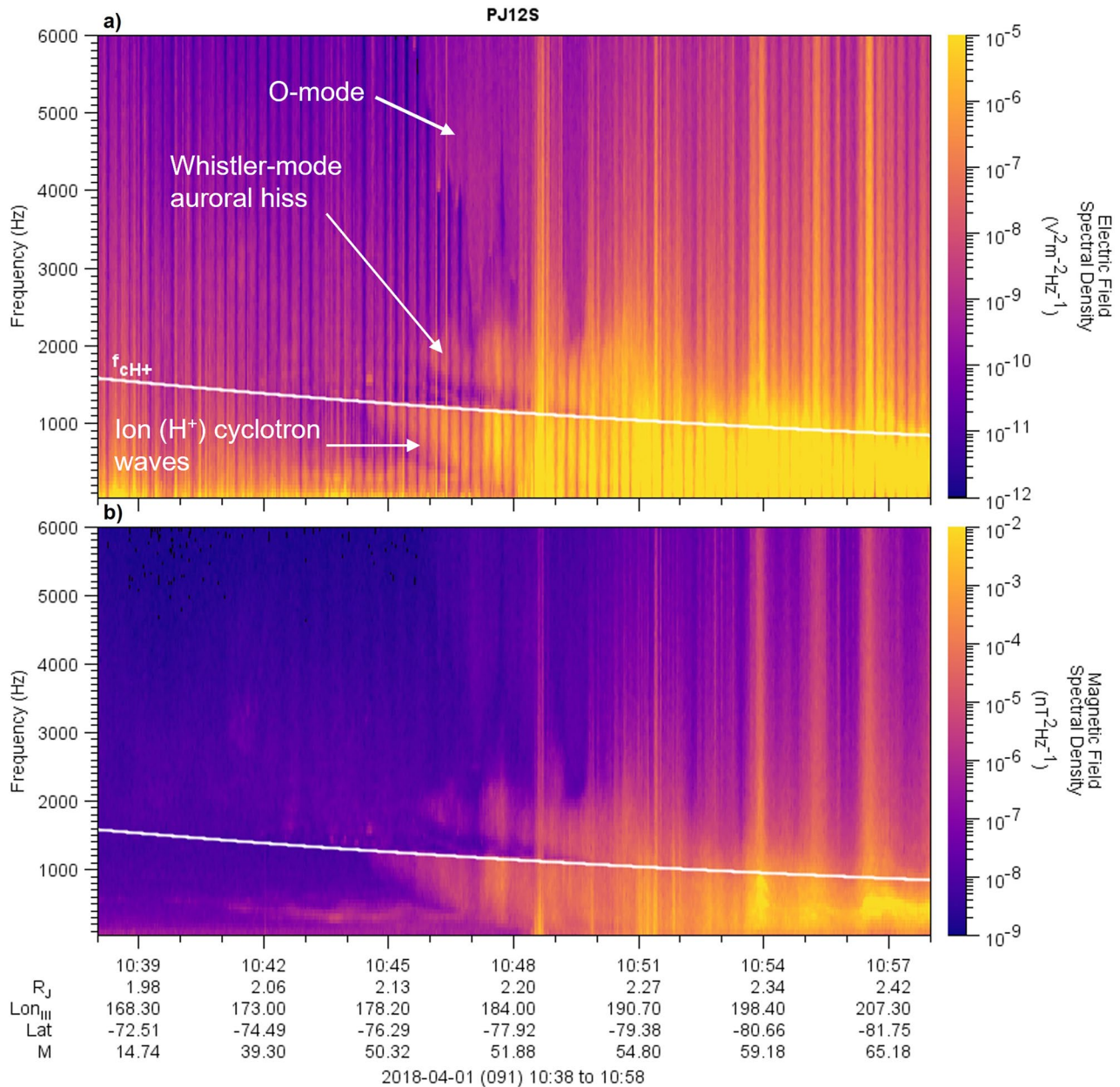
Figure 10. (a) Electric and (b) magnetic field frequency-time spectrograms when Juno was magnetically connected to Jupiter's southern auroral zone near its 12th perijove (PJ12S) showing the characteristic funnel-shaped whistler-mode auroral hiss above f_{cH+}.

6. Low-frequency plasma waves in Zone-II are the most intense. Electromagnetic emissions are also prevalent in Zone-II where broadband energetic electrons peak, which in turn are correlated with deflections in δB_{φ}. These are prevalent in Earth's downward current regions. We demonstrate that they are a result of large-amplitude solitary waves. These have previously been shown to be the stable end-result of a two-stream instability and are capable of supporting potential structures (Matsumoto et al., 1994). We therefore suggest this likely explains their presence in a zone dominated by bidirectional populations.

7. Using plasma wave spectra, large-scale electron density depletions, or auroral cavities, are identified over the auroral zones with an average boundary between the diffuse aurora and Zone-I. These depletions are critical for the development of high-latitude parallel potentials, Alfvénic dissipation, and radio wave generation.
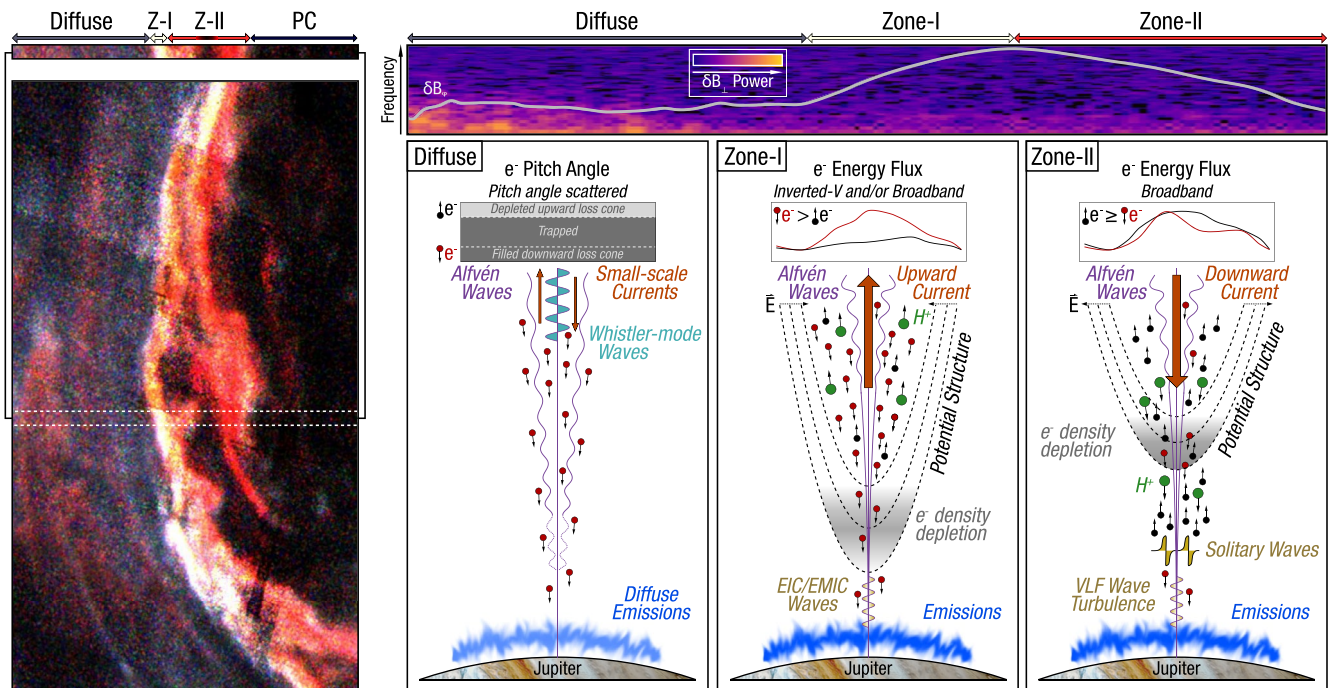
Figure 11. Graphic illustrating the average picture of the fields, particles, and plasma waves in Jupiter's low-altitude diffuse aurora, Zone-I, and Zone-II.

Data Availability Statement

The Waves, JADE, MAG, and JEDI data used in this article have the data set ID JNO-E/J/SS-WAV-3-CDR-BSTFULL-V1.0, JNO-J/SW-JAD-3-CALIBRATED-V1.0, JNO-J-3-FGM-CAL-V1.0, and JNO-J-JED-3-CDR-V1.0, respectively, and are publicly accessible through the Planetary Plasma Interactions Node in the Planetary Data System (https://pds-ppi.igpp.ucla.edu/). In this study, we use an effective E-field antenna length of 0.5 m. The UVS data have data set ID jnouvs_3001 and are publicly accessible through the Atmospheres Node in the Planetary Data System (https://pds-atmospheres.nmsu.edu/).

References

Allegrini, F., Bagenal, F., Bolton, S., Connerney, J., Clark, G., Ebert, R. W., et al. (2017). Electron beams and loss cones in the auroral regions of Jupiter. *Geophysical Research Letters*, *44*(14), 7131–7139. https://doi.org/10.1002/2017GL073180

Allegrini, F., Mauk, B., Clark, G., Gladstone, G. R., Hue, V., Kurth, W. S., et al. (2020). Energy flux and characteristic energy of electrons over Jupiter's main auroral emission. *Journal of Geophysical Research: Space Physics*, *125*(4). https://doi.org/10.1029/2019JA027693

Allegrini, F., Kurth, W. S., Elliott, S. S., Saur, J., Livadiotis, G., Nicolaou, G., et al. (2021). Electron partial density and temperature over Jupiter's main auroral emission using Juno observations. *Journal of Geophysical Research: Space Physics*, *126*(9), e2021JA029426. https://doi.org/10.1029/2021JA029426

André, M., Norqvist, P., Andersson, L., Eliasson, L., Eriksson, A. I., Blomberg, L., et al. (1998). Ion energization mechanisms at 1700 km in the auroral region. *Journal of Geophysical Research*, *103*, A3. https://doi.org/10.1029/97JA00855

Bader, A., Badman, S. V., Ray, L. C., Paranicas, C. P., Lorch, C. T. S., Clark, G., et al. (2020). Energetic particle signatures above Saturn's aurorae. *Journal of Geophysical Research: Space Physics*, *125*(1), e2019JA027403. https://doi.org/10.1029/2019JA027403

Block, L. P., & Fälthammar, C.-G. (1968). Effects of field-aligned currents on the structure of the ionosphere. *Journal of Geophysical Research*, *73*(15), 4807–4812. https://doi.org/10.1029/JA073i015p04807

Bonfond, B., Gladstone, G. R., Grodent, D., Greathouse, T. K., Versteeg, M. H., Hue, V., et al. (2017). Morphology of the UV aurorae Jupiter during Juno's first perijove observations. *Geophysical Research Letters*, *44*(10), 4463–4471. https://doi.org/10.1002/2017GL073114

Bonfond, B., Yao, Z. H., Gladstone, G. R., Grodent, D., Gérard, J.-C., Matar, J., et al. (2021). Are dawn storms Jupiter's auroral substorms? *AGU Advances*, *2*(1), e2020AV000275. https://doi.org/10.1029/2020AV000275

Carlson, C. W., Pfaff, R. F., & Watzin, J. G. (1998). The fast auroral SnapshoT (FAST) mission. *Geophysical Research Letters*, *25*(12), 2013–2016. https://doi.org/10.1029/98GL01592

Cattell, C., Bergmann, R., Sigsbee, K., Carlson, C., Chaston, C., Ergun, R., et al. (1998). The association of electrostatic ion cyclotron waves, ion and electron beams and field-aligned currents: FAST observations of an auroral zone crossing near midnight. *Geophysical Research Letters*, *25*(12), 2053–2056. https://doi.org/10.1029/98GL00834

Chang, T., Crew, G. B., Hershkowitz, N., Jasperse, J. R., Retterer, J. M., & Winningham, J. D. (1986). Transverse acceleration of oxygen ions by electromagnetic ion cyclotron resonance with broad band left-hand polarized waves. *Geophysical Research Letters*, *13*(7), 636–639. https://doi.org/10.1029/GL013i007p00636

Chaston, C. C., Ergun, R. E., Delory, G. T., Peria, W., Temerin, M., Cattell, C., et al. (1998). Characteristics of electromagnetic proton cyclotron waves along auroral field lines observed by FAST in regions of upward current. *Geophysical Research Letters*, *25*(12), 2057–2060. https://doi.org/10.1029/98GL00513

Chaston, C. C., Salem, C., Bonnell, J. W., Carlson, C. W., Ergun, R. E., Strangeway, R. J., & McFadden, J. P. (2008). The turbulent Alfvenic aurora. *Physical Review Letters*, *100*(17), 175003. https://doi.org/10.1103/PhysRevLett.100.175003

Clark, G., Mauk, B. H., Haggerty, D., Paranicas, C., Kollmann, P., Rymer, A., et al. (2017). Energetic particle signatures of magnetic field-aligned potentials over Jupiter's polar regions. *Geophysical Research Letters*, *44*(17), 8703–8711. https://doi.org/10.1002/2017GL074366

Clark, G., Mauk, B. H., Kollmann, P., Szalay, J. R., Sulaiman, A. H., Gershman, D. J., et al. (2020). Energetic proton acceleration associated with Io's footprint tail. *Geophysical Research Letters*, *47*(24), e2020GL090839. https://doi.org/10.1029/2020GL090839

Clark, G., Tao, C., Mauk, B. H., Nichols, J., Saur, J., Bunce, E. J., et al. (2018). Precipitating electron energy flux and characteristic energies in Jupiter's main auroral region as measured by Juno/JEDI. *Journal of Geophysical Research: Space Physics*, *123*(9), 7554–7567. https://doi.org/10.1029/2018JA025639

Connerney, J. E. P., Acuña, M. H., & Ness, N. F. (1981). Modeling the Jovian current sheet and inner magnetosphere. *Journal of Geophysical Research*, *86*(A10), 8370–8384. https://doi.org/10.1029/JA086iA10p08370

Connerney, J. E. P., Benn, M., Bjarno, J. B., Denver, T., Espley, J., Jorgensen, J. L., et al. (2017). The Juno magnetic field investigation. *Space Science Reviews*, *213*(1), 39–138. https://doi.org/10.1007/s11214-017-0334-z

Connerney, J. E. P., Kotsiaros, S., Oliversen, R. J., Espley, J. R., Joergensen, J. L., Joergensen, P. S., et al. (2018). A new model of Jupiter's magnetic field from Juno's first nine orbits. *Geophysical Research Letters*, *45*(6), 2590–2596. https://doi.org/10.1002/2018GL077312

Cowley, S. W. H., & Bunce, E. J. (2001). Origin of the main auroral oval in Jupiter's coupled magnetosphere–ionosphere system. *Planetary and Space Science*, *49*(10–11), 1067–1088. https://doi.org/10.1016/S0032-0633(00)00167-7

Delamere, P. A., & Bagenal, F. (2010). Solar wind interaction with Jupiter's magnetosphere. *Journal of Geophysical Research: Space Physics*, *115*(A10). AA10201. https://doi.org/10.1029/2010JA015347

Ebert, R. W., Allegrini, F., Bagenal, F., Bolton, S. J., Connerney, J. E. P., Clark, G., et al. (2017). Spatial distribution and properties of 0.1–100 keV electrons in Jupiter's polar auroral region. *Geophysical Research Letters*, *44*(18), 9199–9207. https://doi.org/10.1002/2017GL075106

Ebert, R. W., Greathouse, T. K., Clark, G., Hue, V., Allegrini, F., Bagenal, F., et al. (2021). Simultaneous UV images and high-latitude particle and field measurements during an auroral dawn storm at Jupiter. *Journal of Geophysical Research: Space Physics*, e2021JA029679. https://doi.org/10.1029/2021JA029679

Elliott, S. S., Gurnett, D. A., Kurth, W. S., Clark, G., Mauk, B. H., Bolton, S. J., et al. (2018). Pitch angle scattering of upgoing electron beams in Jupiter's polar regions by whistler mode waves. *Geophysical Research Letters*, *45*(3), 1246–1252. https://doi.org/10.1002/2017GL076878

Elliott, S. S., Gurnett, D. A., Kurth, W. S., Mauk, B. H., Ebert, R. W., Clark, G., et al. (2018). The acceleration of electrons to high energies over the Jovian polar cap via whistler mode wave-particle interactions. *Journal of Geophysical Research: Space Physics*, *123*(9), 7523–7533. https://doi.org/10.1029/2018JA025797

Elliott, S. S., Gurnett, D. A., Yoon, P. H., Kurth, W. S., Mauk, B. H., Ebert, R. W., et al. (2020). The generation of upward-propagating whistler mode waves by electron beams in the Jovian polar regions. *Journal of Geophysical Research: Space Physics*, *125*(6), e2020JA027868. https://doi.org/10.1029/2020JA027868

Elliott, S. S., Sulaiman, A. H., Kurth, W. S., Faden, J., Allegrini, F., Valek, P., et al. (2021). The high-latitude extension of Jupiter's Io torus: Electron densities measured by Juno waves. *Journal of Geophysical Research: Space Physics*, *126*(8), e2021JA029195. https://doi.org/10.1029/2021JA029195

Ergun, R. E., Andersson, L., Main, D. S., Su, Y.-J., Carlson, C. W., McFadden, J. P., & Mozer, F. S. (2002). Parallel electric fields in the upward current region of the aurora: Indirect and direct observations. *Physics of Plasmas*, *9*(9), 3685–3694. https://doi.org/10.1063/1.1499120

Ergun, R. E., Carlson, C. W., McFadden, J. P., Mozer, F. S., Delory, G. T., Peria, W., et al. (1998a). FAST satellite observations of electric field structures in the auroral zone. *Geophysical Research Letters*, *25*(12), 2025–2028. https://doi.org/10.1029/98GL00635

Ergun, R. E., Carlson, C. W., McFadden, J. P., Mozer, F. S., Delory, G. T., Peria, W., et al. (1998b). FAST satellite observations of large-amplitude solitary structures. *Geophysical Research Letters*, *25*(12), 2041–2044. https://doi.org/10.1029/98GL00636

Farrell, W. M., Gurnett, D. A., & Goertz, C. K. (1989). Coherent Cerenkov radiation from the Spacelab 2 electron beam. *Journal of Geophysical Research: Space Physics*, *94*(A1), 443–452. https://doi.org/10.1029/JA094iA01p00443

Gershman, D. J., Connerney, J. E. P., Kotsiaros, S., DiBraccio, G. A., Martos, Y. M., Viñas, A. F., et al. (2019). Alfvénic fluctuations associated with Jupiter's auroral emissions. *Geophysical Research Letters*, *46*(13), 7157–7165. https://doi.org/10.1029/2019GL082951

Gladstone, G. R., Persyn, S. C., Eterno, J. S., Walther, B. C., Slater, D. C., Davis, M. W., et al. (2017a). The ultraviolet spectrograph on NASA's Juno mission. *Space Science Reviews*, *213*(1), 447–473. https://doi.org/10.1007/s11214-014-0040-z

Gladstone, G. R., Versteeg, M. H., Greathouse, T. K., Hue, V., Davis, M. W., Gérard, J.-C., et al. (2017b). Juno-UVS approach observations of Jupiter's auroras. *Geophysical Research Letters*, *44*(15), 7668–7675. https://doi.org/10.1002/2017GL073377

Gladstone, G. R., Waite, J. H., Grodent, D., Lewis, W. S., Crary, F. J., Elsner, R. F., et al. (2002). A pulsating auroral X-ray hot spot on Jupiter. *Nature*, *415*(6875), 1000–1003. https://doi.org/10.1038/4151000a

Grodent, D. (2015). A brief review of ultraviolet auroral emissions on giant planets. *Space Science Reviews*, *187*(1), 23–50. https://doi.org/10.1007/s11214-014-0052-8

Gurnett, D. A. (1966). A satellite study of VLF hiss. *Journal of Geophysical Research*, *71*(23), 5599–5615. https://doi.org/10.1029/JZ071i023p05599

Gurnett, D. A., Averkamp, T. F., Schippers, P., Persoon, A. M., Hospodarsky, G. B., Leisner, J. S., et al. (2011). Auroral hiss, electron beams and standing Alfvén wave currents near Saturn's moon Enceladus. *Geophysical Research Letters*, *38*, L06102. https://doi.org/10.1029/2011GL046854

Gurnett, D. A., Huff, R. L., Menietti, J. D., Burch, J. L., Winningham, J. D., & Shawhan, S. D. (1984). Correlated low-frequency electric and magnetic noise along the auroral field lines. *Journal of Geophysical Research: Space Physics*, *89*(A10), 8971–8985. https://doi.org/10.1029/JA089iA10p08971

Gurnett, D. A., & Shaw, R. R. (1973). Electromagnetic radiation trapped in the magnetosphere above the plasma frequency. *Journal of Geophysical Research*, *78*(34), 8136–8149. https://doi.org/10.1029/JA078i034p08136

Gurnett, D. A., Shawhan, S. D., & Shaw, R. R. (1983). Auroral hiss, Z mode radiation, and auroral kilometric radiation in the polar magnetosphere: DE 1 observations. *Journal of Geophysical Research*, *88*, 329–340. https://doi.org/10.1029/JA088iA01p00329

Hill, T. W. (1979). Inertial limit on corotation. *Journal of Geophysical Research: Space Physics*, *84*(A11), 6554–6558. https://doi.org/10.1029/JA084iA11p06554

Hill, T. W. (2001). The Jovian auroral oval. *Journal of Geophysical Research: Space Physics*, *106*(A5), 8101–8107. https://doi.org/10.1029/2000JA000302

Hull, A. J., Bonnell, J. W., Mozer, F. S., & Scudder, J. D. (2003). A statistical study of large-amplitude parallel electric fields in the upward current region of the auroral acceleration region. *Journal of Geophysical Research: Space Physics*, *108*(A1), SMP-51–SMP-523. https://doi.org/10.1029/2001JA007540

Imai, M., Greathouse, T. K., Kurth, W. S., Gladstone, G. R., Louis, C. K., Zarka, P., et al. (2019). Probing Jovian broadband kilometric radio sources tied to the ultraviolet main auroral oval with Juno. *Geophysical Research Letters*, *46*(2), 571–579. https://doi.org/10.1029/2018GL081227

James, H. G. (1976). VLF saucers. *Journal of Geophysical Research*, *81*(4), 501–514. https://doi.org/10.1029/JA081i004p00501

Joy, S. P., Kivelson, M. G., Walker, R. J., Khurana, K. K., Russell, C. T., & Ogino, T. (2002). Probabilistic models of the Jovian magnetopause and bow shock locations. *Journal of Geophysical Research: Space Physics*, *107*(A10), SMP-171–SMP-1717. https://doi.org/10.1029/2001JA009146

Khurana, K. K., Kivelson, M. G., Vasyliunas, V. M., Krupp, N., Woch, J., Lagg, A., et al. (2004). The configuration of Jupiter's magnetosphere. In F. Bagenal, T. E. Dowling, & W. B. McKinnon (Eds.), *Jupiter: The planet, satellites, and magnetosphere* (pp. 593–616). Cambridge University Press.

Kivelson, M. G., & Southwood, D. J. (2005). Dynamical consequences of two modes of centrifugal instability in Jupiter's outer magnetosphere. *Journal of Geophysical Research: Space Physics*, *110*(A12), A12209. https://doi.org/10.1029/2005JA011176

Knight, S. (1973). Parallel electric fields. *Planetary and Space Science*, *21*(5), 741–750. https://doi.org/10.1016/0032-0633(73)90093-7

Kolmašová, I., Imai, M., Santolík, O., Kurth, W. S., Hospodarsky, G. B., Gurnett, D. A., et al. (2018). Discovery of rapid whistlers close to Jupiter implying lightning rates similar to those on Earth. *Nature Astronomy*, *2*(7), 544–548. https://doi.org/10.1038/s41550-018-0442-z

Kotsiaros, S., Connerney, J. E. P., Clark, G., Allegrini, F., Gladstone, G. R., Kurth, W. S., et al. (2019). Birkeland currents in Jupiter's magnetosphere observed by the polar-orbiting Juno spacecraft. *Nature Astronomy*, *3*(10), 904–909. https://doi.org/10.1038/s41550-019-0819-7

Kurth, W. S., Hospodarsky, G. B., Kirchner, D. L., Mokrzycki, B. T., Averkamp, T. F., Robison, W. T., et al. (2017). The Juno waves investigation. *Space Science Reviews*, *213*(1), 347–392. https://doi.org/10.1007/s11214-017-0396-y

Kurth, W. S., Imai, M., Hospodarsky, G. B., Gurnett, D. A., Louarn, P., Valek, P., et al. (2017). A new view of Jupiter's auroral radio spectrum. *Geophysical Research Letters*, *44*(14), 7114–7121. https://doi.org/10.1002/2017GL072889

Kurth, W. S., Mauk, B. H., Elliott, S. S., Gurnett, D. A., Hospodarsky, G. B., Santolik, O., et al. (2018). Whistler mode waves associated with broadband Auroral electron precipitation at Jupiter. *Geophysical Research Letters*, *45*(18), 9372–9379. https://doi.org/10.1029/2018GL078566

Li, W., Ma, Q., Shen, X.-C., Zhang, X.-J., Mauk, B. H., Clark, G., et al. (2021). Quantification of diffuse auroral electron precipitation driven by whistler mode waves at Jupiter. *Geophysical Research Letters*, *48*(19), e2021GL095457. https://doi.org/10.1029/2021GL095457

Louarn, P., Allegrini, F., McComas, D. J., Valek, P. W., Kurth, W. S., André, N., et al. (2017). Generation of the Jovian hectometric radiation: First lessons from Juno: Juno observations in a HOM radio source. *Geophysical Research Letters*, *44*(10), 4439–4446. https://doi.org/10.1002/2017GL072923

Louis, C. K., Prangé, R., Lamy, L., Zarka, P., Imai, M., Kurth, W. S., & Connerney, J. E. P. (2019). Jovian auroral radio sources detected in situ by Juno/waves: Comparisons with model auroral ovals and simultaneous HST FUV images. *Geophysical Research Letters*, *46*(21), 11606–11614. https://doi.org/10.1029/2019GL084799

Lysak, R. L. (1986). Ion acceleration by wave-particle interaction. In *Ion acceleration in the magnetosphere and ionosphere* (pp. 261–270). American Geophysical Union (AGU). https://doi.org/10.1029/GM038p0261

Lysak, R. L. (1991). Feedback instability of the ionospheric resonant cavity. *Journal of Geophysical Research: Space Physics*, *96*(A2), 1553–1568. https://doi.org/10.1029/90JA02154

Lysak, R. L., Song, Y., Elliott, S., Kurth, W., Sulaiman, A. H., & Gershman, D. (2021). The Jovian ionospheric Alfvén resonator and auroral particle acceleration. *Journal of Geophysical Research: Space Physics*, *126*(12), e2021JA029886. https://doi.org/10.1029/2021JA029886

Maggs, J. E. (1989). Nonlinear evolution of the auroral electron beam. *Journal of Geophysical Research*, *94*(A4), 3631–3651. https://doi.org/10.1029/JA094iA04p03631

Masters, A. (2017). Model-based assessments of magnetic reconnection and Kelvin-Helmholtz instability at Jupiter's magnetopause. *Journal of Geophysical Research: Space Physics*, *122*(11), 11154–11174. https://doi.org/10.1002/2017JA024736

Masters, A. (2018). A more viscous-like solar wind interaction with all the giant planets. *Geophysical Research Letters*, *45*(15), 7320–7329. https://doi.org/10.1029/2018GL078416

Masters, A., Dunn, W. R., Stallard, T. S., Manners, H., & Stawarz, J. (2021). Magnetic reconnection near the planet as a possible driver of Jupiter's mysterious polar auroras. *Journal of Geophysical Research: Space Physics*, *126*(8), e2021JA029544. https://doi.org/10.1029/2021JA029544

Matsumoto, H., Kojima, H., Miyatake, T., Omura, Y., Okada, M., Nagano, I., & Tsutsui, M. (1994). Electrostatic solitary waves (ESW) in the magnetotail: BEN wave forms observed by GEOTAIL. *Geophysical Research Letters*, *21*(25), 2915–2918. https://doi.org/10.1029/94GL01284

Mauk, B. H., Clark, G., Gladstone, G. R., Kotsiaros, S., Adriani, A., Allegrini, F., et al. (2020). Energetic particles and acceleration regions over Jupiter's polar cap and main aurora: A broad overview. *Journal of Geophysical Research: Space Physics*, *125*(3), e2019JA027699. https://doi.org/10.1029/2019JA027699

Mauk, B. H., Haggerty, D. K., Jaskulek, S. E., Schlemm, C. E., Brown, L. E., Cooper, S. A., et al. (2017). The Jupiter energetic particle detector instrument (JEDI) investigation for the Juno mission. *Space Science Reviews*, *213*(1), 289–346. https://doi.org/10.1007/s11214-013-0025-3

Mauk, B. H., Haggerty, D. K., Paranicas, C., Clark, G., Kollmann, P., Rymer, A. M., et al. (2017a). Juno observations of energetic charged particles over Jupiter's polar regions: Analysis of monodirectional and bidirectional electron beams. *Geophysical Research Letters*, *44*(10), 4410–4418. https://doi.org/10.1002/2016GL072286

Mauk, B. H., Haggerty, D. K., Paranicas, C., Clark, G., Kollmann, P., Rymer, A. M., et al. (2017b). Discrete and broadband electron acceleration in Jupiter's powerful aurora. *Nature*, *549*(7670), 66–69. https://doi.org/10.1038/nature23648

Mauk, B. H., Haggerty, D. K., Paranicas, C., Clark, G., Kollmann, P., Rymer, A. M., et al. (2018). Diverse electron and ion acceleration characteristics observed over Jupiter's main aurora. *Geophysical Research Letters*, *45*(3), 1277–1285. https://doi.org/10.1002/2017GL076901

McComas, D. J., Alexander, N., Allegrini, F., Bagenal, F., Beebe, C., Clark, G., et al. (2017). The Jovian Auroral Distributions Experiment (JADE) on the Juno mission to Jupiter. *Space Science Reviews*, *213*(1), 547–643. https://doi.org/10.1007/s11214-013-9990-9

McComas, D. J., & Bagenal, F. (2007). Jupiter: A fundamentally different magnetospheric interaction with the solar wind. *Geophysical Research Letters*, *34*(20), L20106. https://doi.org/10.1029/2007GL031078

McFadden, J. P., Carlson, C. W., Ergun, R. E., Chaston, C. C., Mozer, F. S., Temerin, M., et al. (1998). Electron modulation and ion cyclotron waves observed by FAST. *Geophysical Research Letters*, *25*(12), 2045–2048. https://doi.org/10.1029/98GL00855

McIlwain, C. E. (1961). Coordinates for mapping the distribution of magnetically trapped particles. *Journal of Geophysical Research*, *66*, 3681–3691. https://doi.org/10.1029/JZ066i011p03681

Mitchell, D. G., Kurth, W. S., Hospodarsky, G. B., Krupp, N., Saur, J., Mauk, B. H., et al. (2009). Ion conics and electron beams associated with auroral processes on Saturn. *Journal of Geophysical Research: Space Physics*, *114*(A2), A02212. https://doi.org/10.1029/2008JA013621

Mura, A., Adriani, A., Altieri, F., Connerney, J. E. P., Bolton, S. J., Moriconi, M. L., et al. (2017). Infrared observations of Jovian aurora from Juno's first orbits: Main oval and satellite footprints. *Geophysical Research Letters*, *44*(11), 5308–5316. https://doi.org/10.1002/2017GL072954

Nichols, J. D., & Cowley, S. W. H. (2004). Magnetosphere-ionosphere coupling currents in Jupiter's middle magnetosphere: Effect of precipitation-induced enhancement of the ionospheric Pedersen conductivity. *Annales Geophysica*e, 22(5), 1799–1827. https://doi.org/10.5194/angeo-22-1799-2004

Paranicas, C., Mauk, B. H., Haggerty, D. K., Clark, G., Kollmann, P., Rymer, A. M., et al. (2018). Intervals of intense energetic electron beams over Jupiter's Poles. *Journal of Geophysical Research: Space Physics*, 123(3), 1989–1999. https://doi.org/10.1002/2017JA025106

Paschmann, G., Haaland, S., & Treumann, R. (2003). The aurora as a universal phenomenon. In G. Paschmann, S. Haaland, & R. Treumann (Eds.), *Auroral plasma physic*s (pp. 415–434). Springer Netherlands. https://doi.org/10.1007/978-94-007-1086-3_9

Persoon, A. M., Gurnett, D. A., Peterson, W. K., Waite, J. H., Jr., Burch, J. L., & Green, J. L. (1988). Electron density depletions in the nightside auroral zone. *Journal of Geophysical Research: Space Physics*, 93(A3), 1871–1895. https://doi.org/10.1029/JA093iA03p01871

Persoon, A. M., Kurth, W. S., Gurnett, D. A., Groene, J. B., Sulaiman, A. H., Wahlund, J.-E., et al. (2019). Electron density distributions in Saturn's ionosphere. *Geophysical Research Letters*, 46(6), 3061–3068. https://doi.org/10.1029/2018GL078020

Rankin, R., Samson, J. C., Tikhonchuk, V. T., & Voronkov, I. (1999). Auroral density fluctuations on dispersive field line resonances. *Journal of Geophysical Research: Space Physics*, 104(A3), 4399–4410. https://doi.org/10.1029/1998JA900106

Ray, L. C., Ergun, R. E., Delamere, P. A., & Bagenal, F. (2010). Magnetosphere-ionosphere coupling at Jupiter: Effect of field-aligned potentials on angular momentum transport. *Journal of Geophysical Research: Space Physics*, 115(A9), A09211. https://doi.org/10.1029/2010JA015423

Ray, L. C., Su, Y.-J., Ergun, R. E., Delamere, P. A., & Bagenal, F. (2009). Current-voltage relation of a centrifugally confined plasma. *Journal of Geophysical Research: Space Physics*, 114(A4), A04214. https://doi.org/10.1029/2008JA013969

Santolík, O., & Gurnett, D. A. (2002). Propagation of auroral hiss at high altitudes: Propagation of auroral hiss at high altitudes. *Geophysical Research Letters*, 29(10), 1191–1194. https://doi.org/10.1029/2001GL013666

Santolík, O., Parrot, M., & Němec, F. (2016). Propagation of equatorial noise to low altitudes: Decoupling from the magnetosonic mode. *Geophysical Research Letters*, 43, 13. https://doi.org/10.1002/2016GL069582

Saur, J., Janser, S., Schreiner, A., Clark, G., Mauk, B. H., Kollmann, P., et al. (2018). Wave-particle interaction of Alfvén waves in Jupiter's magnetosphere: Auroral and magnetospheric particle acceleration. *Journal of Geophysical Research: Space Physics*, 123(11), 9560–9573. https://doi.org/10.1029/2018JA025948

Saur, J., Politano, H., Pouquet, A., & Matthaeus, W. H. (2002). Evidence for weak MHD turbulence in the middle magnetosphere of Jupiter. *Astronomy & Astrophysics*, 386(2), 699–708. https://doi.org/10.1051/0004-6361:20020305

Saur, J., Pouquet, A., & Matthaeus, W. H. (2003). An acceleration mechanism for the generation of the main auroral oval on Jupiter. *Geophysical Research Letters*, 30(5), 1260. https://doi.org/10.1029/2002GL015761

Shi, C., Zhao, J., Sun, H., Huang, C., & Xie, H. (2020). Electromagnetic emission driven by electron beam instability in the Jovian polar regions. *The Astrophysical Journal*, 902(2), 151. https://doi.org/10.3847/1538-4357/abb5a1

Song, Y., & Lysak, R. L. (2006). Displacement current and the generation of parallel electric fields. *Physical Review Letters*, 96(14), 145002. https://doi.org/10.1103/PhysRevLett.96.145002

Sulaiman, A. H., Elliott, S. S., Kurth, W. S., Faden, J. B., Hospodarsky, G. B., & Menietti, J. D. (2021). Inferring Jovian electron densities using plasma wave spectra obtained by the Juno/waves instrument. *Journal of Geophysical Research: Space Physics*, 126(8), e2021JA029263. https://doi.org/10.1029/2021JA029263

Sulaiman, A. H., Hospodarsky, G. B., Elliott, S. S., Kurth, W. S., Gurnett, D. A., Imai, M., et al. (2020). Wave-particle interactions associated with Io's auroral footprint: Evidence of Alfvén, ion cyclotron, and whistler modes. *Geophysical Research Letters*, 47(22), e2020GL088432. https://doi.org/10.1029/2020GL088432

Sulaiman, A. H., Kurth, W. S., Hospodarsky, G. B., Averkamp, T. F., Ye, S.-Y., Menietti, J. D., et al. (2018). Enceladus auroral hiss emissions during Cassini's Grand Finale. *Geophysical Research Letters*, 45(15), 7347–7353. https://doi.org/10.1029/2018GL078130

Szalay, J. R., Allegrini, F., Bagenal, F., Bolton, S. J., Clark, G., Connerney, J. E. P., et al. (2017). Plasma measurements in the Jovian polar region with Juno/JADE. *Geophysical Research Letters*, 86(A8), 8447–8449. https://doi.org/10.1002/2017GL072837

Szalay, J. R., Allegrini, F., Bagenal, F., Bolton, S. J., Clark, G., Connerney, J. E. P., et al. (2021). Proton outflow associated with Jupiter's auroral processes. *Geophysical Research Letters*, 48(1), e2020GL091627. https://doi.org/10.1029/2C627

Szalay, J. R., Clark, G., Livadiotis, G., McComas, D. J., Mitchell, D. G., Rankin, J. S., et al. (2022). Closed fluxtubes and dispersive proton conics at Jupiter's polar cap. *Geophysical Research Letters*, 49(9), e2022GL098741. https://doi.org/10.1029/2022GL098741

Temerin, M., Cerny, K., Lotko, W., & Mozer, F. S. (1982). Observations of double layers and solitary waves in the auroral plasma. *Physical Review Letters*, 48(17), 1175–1179. https://doi.org/10.1103/PhysRevLett.48.1175

Thomas, N., Bagenal, F., Hill, T. W., & Wilson, J. K. (2004). The Io neutral clouds and plasma torus. In F. Bagenal, T. E. Dowling, & W. B. McKinnon (Eds.), *Jupiter: The planet, satellites, and magnetosphere* (pp. 593–616). Cambridge University Press.

Waite, J. H., Gladstone, G. R., Lewis, W. S., Goldstein, R., McComas, D. J., Riley, P., et al. (2001). An auroral flare at Jupiter. *Nature*, 410(6830), 787–789. https://doi.org/10.1038/35071018

Wu, C. S., & Lee, L. C. (1979). A theory of the terrestrial kilometric radiation. *The Astrophysical Journal*, 230, 621–626. https://doi.org/10.1086/157120

Zhang, B., Delamere, P. A., Yao, Z., Bonfond, B., Lin, D., Sorathia, K. A., et al. (2021). How Jupiter's unusual magnetospheric topology structures its aurora. *Science Advances*, 7(15), eabd1204. https://doi.org/10.1126/sciadv.abd1204